



# Metallogenesis of the Huangtan Au–Cu–Zn deposit in East Tianshan, NW China: constraints from isotopes (H, O, He, Ar, and S) and Re–Os geochronology

Zhenlong Zhang<sup>1,2</sup> · Xinxia Geng<sup>1</sup> · Zhixin Zhang<sup>3</sup> · Fuquan Yang<sup>1</sup> · Qiangfen Xu<sup>4</sup> · Chengdong Yang<sup>1</sup>

Received: 28 January 2021 / Accepted: 13 November 2021 / Published online: 4 January 2022  
© Geologische Vereinigung e.V. (GV) 2021

## Abstract

The Huangtan (including Jinling) Au–Cu–Zn deposit is an auriferous volcanogenic massive sulfide (VMS) deposit discovered in East Tianshan, Central Asian Orogenic Belt. The deposit is hosted in volcanic breccia and tuff of the Silurian Hongliuxia Formation. The ore bodies consist of concordant massive sulfide lenses and discordant sulfide veins. Chalcopyrite Re–Os dating constrained the age of mineralization in the Huangtan deposit at 432 Ma. Quartz and barite host abundant liquid-rich, liquid-only and minor vapor-rich aqueous fluid inclusions. The fluid inclusions in barite from the exhalative–sedimentary units mainly have homogenization temperatures at 140–260 °C, and calculated salinities of 3–9 wt% NaCl equiv.; Those values are at 120–300 °C, and 1–9 wt% NaCl equiv. for varieties in quartz from the vein ores and alteration assemblages. Fluid inclusions extract from pyrite have  $^3\text{He}/^4\text{He}$  ratios of 0.929–1.374 Ra,  $^{40}\text{Ar}/^{36}\text{Ar}$  of 388–520, and  $^{40}\text{Ar}/^4\text{He}$  of 0.355–0.836. The quartz and barite yielded  $\delta^{18}\text{O}$  values of 7.4‰ to 10.1‰ and the  $\delta\text{D}_{\text{V-SMOW}}$  values of the fluid inclusions in the quartz and barite range from –69 to –42‰. The He–Ar and H–O isotopes imply that the ore-forming fluids were derived from a magmatic source with the addition of deeply circulating seawater. The  $\delta^{34}\text{S}_{\text{V-CDT}}$  values of pyrite and chalcopyrite range from –2.0 to 1.5‰, and those of barite samples range from 24.1 to 24.8‰, which indicates that sulfur was derived from magmatic sulfur, and was subjected to fractionation between sulfide and sulfate. Linked to the ore geology, geochronology data, isotope compositions and fluid inclusions obtained in this study with those of previously published adjacent VMS deposits in the Kalatag area suggest that the Huangtan deposit and adjacent VMS deposits formed in the same metallogenic system.

**Keywords** Auriferous VMS-type mineralization · Stable isotopes · Metallogenesis · Huangtan deposit · East Tianshan

## Introduction

Volcanogenic massive sulfide (VMS) deposits are strata-bound accumulations of sulfide minerals that precipitated at or near the seafloor in spatial, temporal and genetic

association with contemporaneous volcanism. They are one of the most important sources of metals (Zn, Cu, Pb, Ag and Au) in the world (Franklin et al. 2005). VMS deposits contain variable amounts of Au, and a large proportion of deposits are characterized by relatively low Au grades (< 2 g/t). According to the grade of gold and/or gold-to-base metal ratio or amounts of gold, the deposits are classified into auriferous, Au-rich and anomalous VMS deposits (Mercier-Langevin et al. 2011). The Central Asian Orogenic Belt (CAOB) is a large Phanerozoic accretionary orogen situated between the Siberian Craton to the north and the Tarim–North China Craton to the south (Han et al. 2006a; Xiao et al. 2014, 2015; Deng et al. 2017; Yang et al. 2018b). The Altay orogenic belt is located in the CAOB, which is a well-known VMS polymetallic Cu metallogenic belt. There are Au-rich VMS deposits, including Leninogorskoye, Souvenir, and Zarechenskoye in the Kazakhstan and Russia Altay Orogenic Belts (Daukeev et al. 2004; Franklin et al.

✉ Fuquan Yang  
yangfuquan66@sina.com

<sup>1</sup> MNR Key Laboratory of Metallogeny and Mineral Assessment, Institute of Mineral Resources, Chinese Academy of Geological Sciences, Beijing 100037, China  
<sup>2</sup> School of Resources and Environmental Engineering, Hefei University of Technology, Hefei 230009, Anhui, China  
<sup>3</sup> Xinjiang Research Center for Mineral Resources, Xinjiang Institute of Ecology and Geography, Chinese Academy of Sciences, Urumqi 830011, Xinjiang, China  
<sup>4</sup> Geophysical Prospecting Team, Nonferrous Geoexploration Bureau, Urumqi 830000, Xinjiang, China

2005; Yakubchuk et al. 2005; Mercier-Langevin et al. 2011; Lobanov et al. 2014).

The East Tianshan Orogenic Belt is a component of the CAOB in Xinjiang, NW China, which is bordered by the Tarim Basin to the south and the Turpan–Hami Basin to the north (Fig. 1; Sengör et al. 1993; Han and Zhao 2003; Wang et al. 2006; Windley et al. 2007; Xiao et al. 2013). The East Tianshan Orogenic Belt hosts many significant types of metal deposits, such as porphyry Cu deposits (Han et al. 2006b; Wang et al. 2018a), skarn W(–Mo) deposits (Deng et al. 2017; Li et al. 2020), and magmatic Cu–Ni sulfide deposits (Qin et al. 2011; Mao et al. 2015a). Only a few VMS-type deposits have been reported in the East Tianshan Orogenic Belt including Xiaorequanzi and Honghai–Huangtupo VMS Cu–Zn deposits (Deng et al. 2016; Mao et al. 2020). To date, no Au-rich/auriferous VMS deposits have been detected in the East Tianshan Orogenic Belt. The Kalatag area belongs

to the Dananhu arc belt located in the northern part of the East Tianshan Orogenic Belt. The Kalatag area hosts many metal deposits, including the Hongshi (Cheng et al. 2019), Meiling (Yu et al. 2019, 2020), Honghai–Huangtupo (Yang et al. 2018a; Cheng et al. 2020a), Yudai (Chen et al. 2017; Sun et al. 2018), Yueyawan and Xierqu deposits (Mao et al. 2018; Chen et al. 2020; Sun et al. 2019). The Huangtan (including Jinling) Au–Cu–Zn deposit is a newly discovered deposit in the Kalatag area (Liang 2018; Deng et al. 2018a). The Huangtan deposit is located approximately 2 km southeast of the Honghai–Huangtupo deposit. Liang (2018) reported the mineralization features and wall rock alteration of the Huangtan Au–Cu–Zn deposit and suggested that the deposit is best classified as a volcanic hydrothermal type with moderate-to-low-temperature deposits. Based on the analysis of the geological features of the deposit, Deng et al. (2018a) considered the Huangtan deposit to be a typical

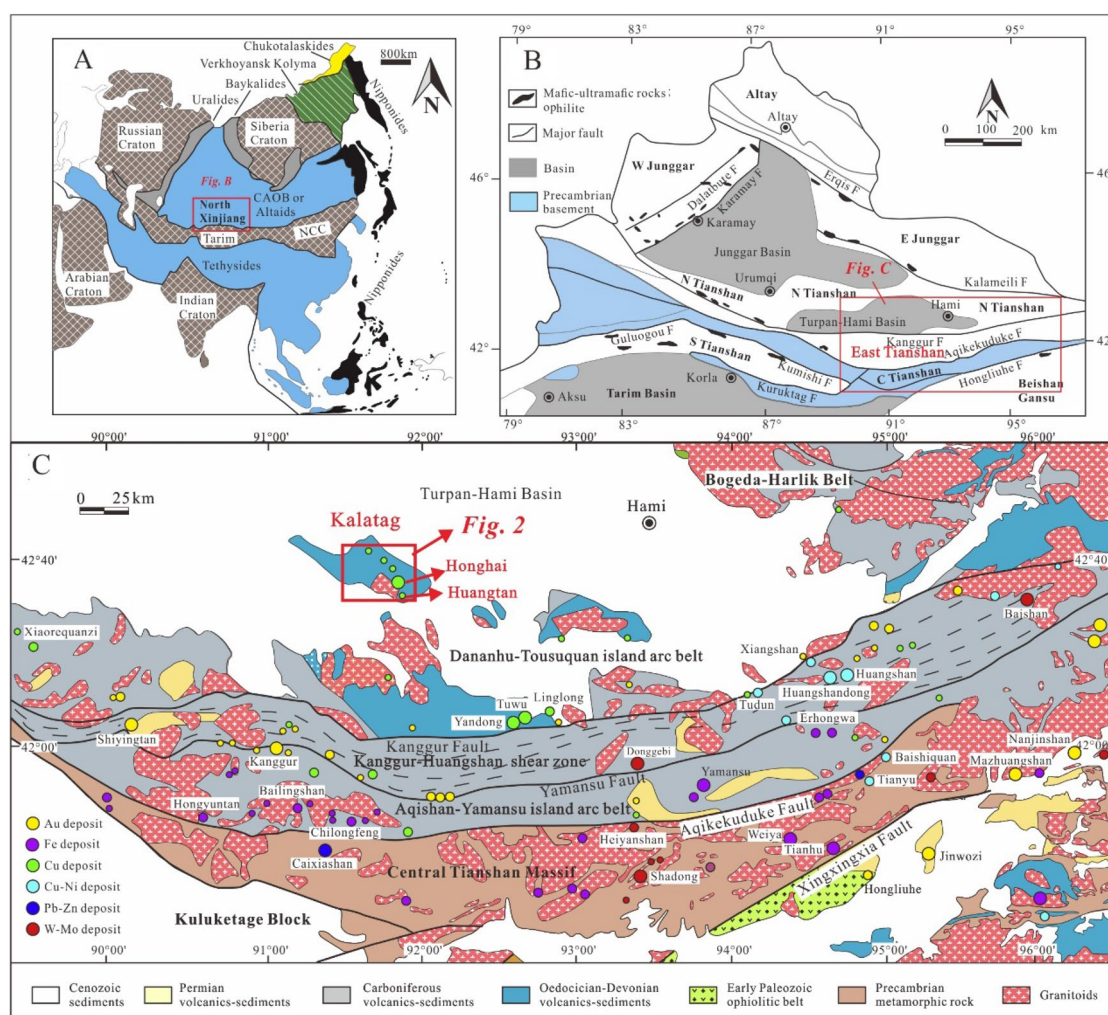


**Fig. 1** A Sketch map showing the location of Northern Xinjiang (modified after Sengör et al. 1993; Xiao et al. 2004). B Sketch map showing the distribution of tectonic units in Northern Xinjiang (mod-

ified after Chen et al. 2012). C Tectonic framework and distribution of ore deposits in the East Tianshan orogen (modified after Deng et al. 2016)

remobilized VMS deposit that was overprinted by subsequent hydrothermal treatment. He (2019) considered that the mineralization process of the Huangtan deposit can be divided into a VMS period and a hydrothermal period. The Re–Os isochron ages of the VMS period, and hydrothermal period are  $436.2 \pm 7.5$ , and  $436.3 \pm 7.6$  Ma, respectively. Sun et al. (2020) argued that the Huangtan igneous rocks were generated by the northward subduction of the North Tianshan oceanic plate beneath the Dananhu–Harlik island arc during the Early Paleozoic. Although several studies on the Huangtan deposit have been carried out, numerous topics require further work, including the origin and evolution of the ore-forming fluids, metallogenic time and metallogenesis. Moreover, whether this deposit in Xinjiang is an auriferous VMS deposit remains unclear.

In this contribution, we analyzed the Re–Os isochron age, fluid inclusions, H–O isotopes, He–Ar isotopes, and S isotopes of the deposit to clarify the origin and evolution of the ore-forming fluids for the Huangtan Au–Cu–Zn deposit and to discuss its metallogenesis. This information will provide new insights for fundamental research and exploration in the East Tianshan Orogenic Belt.

## Geological setting

The East Tianshan Orogenic Belt consists of three tectonic units from south to north, namely, the Central Tianshan massif, Jueluotage belt and Bogeda–Harlik belt, which are separated by the Aqikekuduke and Kalamaili faults (Qin et al. 2011). The Jueluotage belt can be further divided into the Dananhu–Tousuquan island arc belt, Kanggur–Huangshan ductile shear zone and Aqishan–Yamansu island arc belt by the Yamansu and Kangguer faults (Wang et al. 2006; Xiao et al. 2015). The Huangtan deposit is located in the Dananhu–Tousuquan island arc belt. The Dananhu–Tousuquan island arc belt is an intraoceanic arc (Wang and Zhang 2016; Xiao et al. 2017; Wang et al. 2018b; Mao et al. 2019) that is mainly composed of Ordovician to Carboniferous volcanic-sedimentary rocks (BGMRXUAR 1993). The Kanggur–Huangshan ductile shear zone consists of Carboniferous sedimentary and volcanic rocks (Li et al. 2003; Chen et al. 2019). The Yamansu island arc belt is composed mainly of Carboniferous basalt and andesite (Hou et al. 2006; Luo et al. 2016).

The Kalatag area is located in the central part of the Dananhu–Tousuquan island arc belt, which exposes mainly Paleozoic lithologies that include the Ordovician–Silurian Daliugou, Silurian Hongliuxia and Kalatag, Devonian Dananhu, Carboniferous Qishan, and Permian Arbasay formations (Fig. 2). Early Paleozoic volcanic rocks developed in the eastern part of the Kalatag area, and can be subdivided, from bottom to top, into three units. The Daliugou

Formation (Unit 1) is dominated by basalt, basaltic andesite and andesite, which host the volcano-hydrothermal vein Cu deposit (Hongshi); The Hongliuxia Formation (Unit 2) consists of tuffaceous sediments, volcanic breccia, and tuff breccia, which host the VMS deposits (such as the Honghai–Huangtupo and Huangtan deposits, Deng et al. 2018a; Yang et al. 2018a; Cheng et al. 2020a). The Kalatag Formation (Unit 3) is mainly composed of tuff and dacite (Deng et al. 2020). The published geochronological data for these three units span a wide range from 416 Ma to > 446 Ma (Mao et al. 2010; Yu 2014; Deng et al. 2018b, c; Li et al. 2016; Long et al. 2017; Xu 2017; Chai et al. 2019; Mao et al. 2019; Cheng et al. 2020a). The Devonian Dananhu Formation, which unconformably overlies the Early Silurian strata, is dominated by tuff, tuffaceous sandstone and limestone intercalated with andesite. The Carboniferous Qishan and Permian Arbasay formations unconformably overlie the previously mentioned rocks and are dominated by mafic-to-felsic volcanic rocks. The faults are developed in the Kalatag area, including the NWW-trending Kalatag Fault and the EW-trending Kabei Fault. The distribution of volcanism and mineralization in the Kalatag area are controlled by NNW-, NWW-, and NE-trending faults, which are interpreted as a subsidiary fault system of the Kalatag Fault (Deng et al. 2016).

Magmatic intrusions are widespread in the Kalatag area. The (quartz) diorite porphyry exposed in the Yudai, Xierqu, and Dongerqu ore districts intruded during two episodes: 453–437 Ma and 400–380 Ma (Li et al. 2006; Long et al. 2016; Mao et al. 2018; Sun et al. 2018). The Kalatag pluton in the southeastern part of the Kalatag area is composed of tonalite, diorite, granodiorite, granite, and monzogranite, which have zircon U–Pb ages of 426–440 Ma (Mao 2014; Zheng et al. 2018; Cheng et al. 2020b). Carboniferous magmatism produced quartz porphyry in the Meiling ore district which yields a zircon U–Pb age of 300 Ma (Mao 2014; Yu et al. 2019). The Permian mafic–ultramafic intrusions are composed of troctolite, olivine gabbro, hornblende gabbro, and gabbro in the Yueyawan ore district, which has a zircon U–Pb age of 282 Ma (Sun et al. 2019).

## Deposit geology

### Stratigraphy and intrusive rock

The Huangtan Au–Cu–Zn deposit adjoins the Honghai–Huangtupo Cu–Zn deposit to the northwest. The exposed strata include the Early Paleozoic volcanic rocks and are divided into three units (Fig. 3). Unit 1 (Daliugou Formation), in the southern part of the deposit, is composed of tuff, andesite, basalt, and breccia-bearing andesite. Unit 2 (Hongliuxia Formation), in the central and midwestern

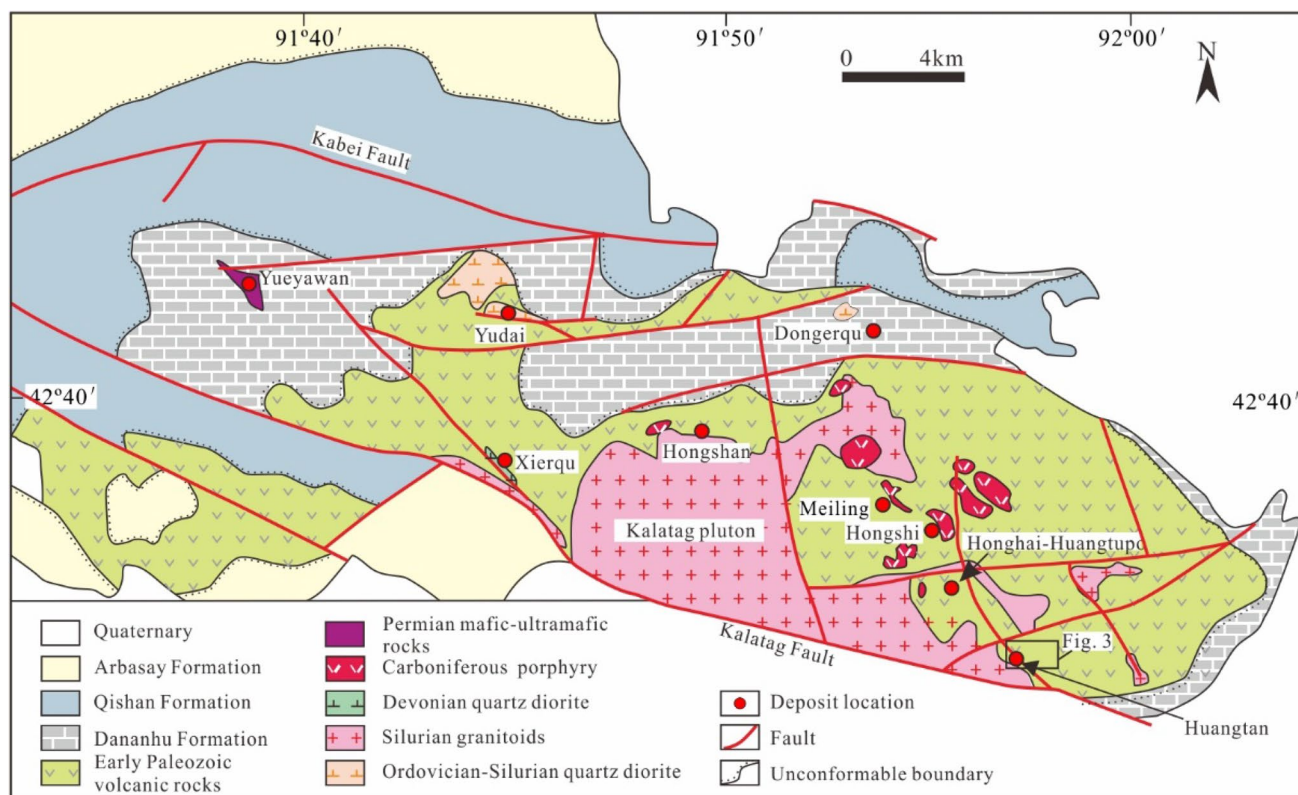


**Fig. 2** Sketch map of the geology and the distribution of ore deposits in the Kalatag area (modified after Deng et al. 2016)

parts of the ore district, mainly consists of dacite, rhyolite, volcanic breccia, and tuff. It primarily hosts the mineralization of the Huangtan Au–Cu–Zn deposit, with volcanic breccia and tuff as the surrounding rocks. Unit 3 (Kalatag Formation), in the northeastern part of the ore district, is mainly composed of andesite, dacite, volcanic breccia, and dacitic tuff.

Diorite and granodiorite dikes are exposed in the western and southwestern parts of the ore district and intrude the Early Paleozoic strata.

### Orebody

In total, 34 ore bodies (not exposed at the surface) are observed in the Huangtan Au–Cu–Zn deposit, including 8 Au ore bodies, 7 Cu ore bodies, 10 Zn ore bodies, 2 Au–Cu ore bodies, 4 Cu–Zn ore bodies, and 3 Au–Cu–Zn ore bodies. The sizes of the orebodies vary; the strike lengths of the orebodies are 50–400 m; and the thicknesses of the orebody are 0.82–40.81 m. The AuCu1 orebody and CuZn2 orebody are principal orebodies. The AuCu1 orebody has average grades of 4.07 g/t Au and 0.78% Cu, and the CuZn2 orebody has average grades of 2.10% Zn and 0.47% Cu. The orebodies are divided into western and eastern sections by the 5150 prospecting line. The orebodies of the western

section generally dip  $196^\circ$  at angles of  $62\text{--}72^\circ$ . The orebodies of the eastern section generally dip  $12\text{--}14^\circ$  at angles of  $10\text{--}41^\circ$  (Fig. 4; XXMCL 2019). These orebodies consist of two parts: concordant massive sulfide lenses and discordant vein-type sulfide mineralization. The concordant massive sulfide lens consists of exhalative–sedimentary units with layered and layered-like shapes (Fig. 5A–F, I). Vein-type sulfide mineralization and altered wall rock are located mainly in footwall strata that are commonly referred to as stockwork units (Fig. 5A–C, G, H, J, L, M). The orebodies detected thus far are dominated by vein-type sulfide mineralization, followed by stratiform mineralization.

The ore structures of massive sulfide lenses include dense massive, banded, and ribbon structures. The ore structures of vein-type sulfide mineralization include disseminated, stockwork, and veinlet structures. The main textures of the ores are euhedral to subhedral granular, anhedral granular, interstitial, poikilitic, exsolution and metasomatic. Metallic minerals include pyrite, chalcopyrite, sphalerite, galena, tennantite, tetrahedrite, and telluride (Fig. 6A–I). Gold in the Huangtan deposit is present in three main mineralogical forms: (1) native gold (Fig. 6D, E), (2) auriferous tellurides (Fig. 6E, H, I), and (3) “invisible” gold. Native gold is present as fine grains in pyrite, chalcopyrite, and quartz. Auriferous tellurides form fine grains in pyrite, quartz,

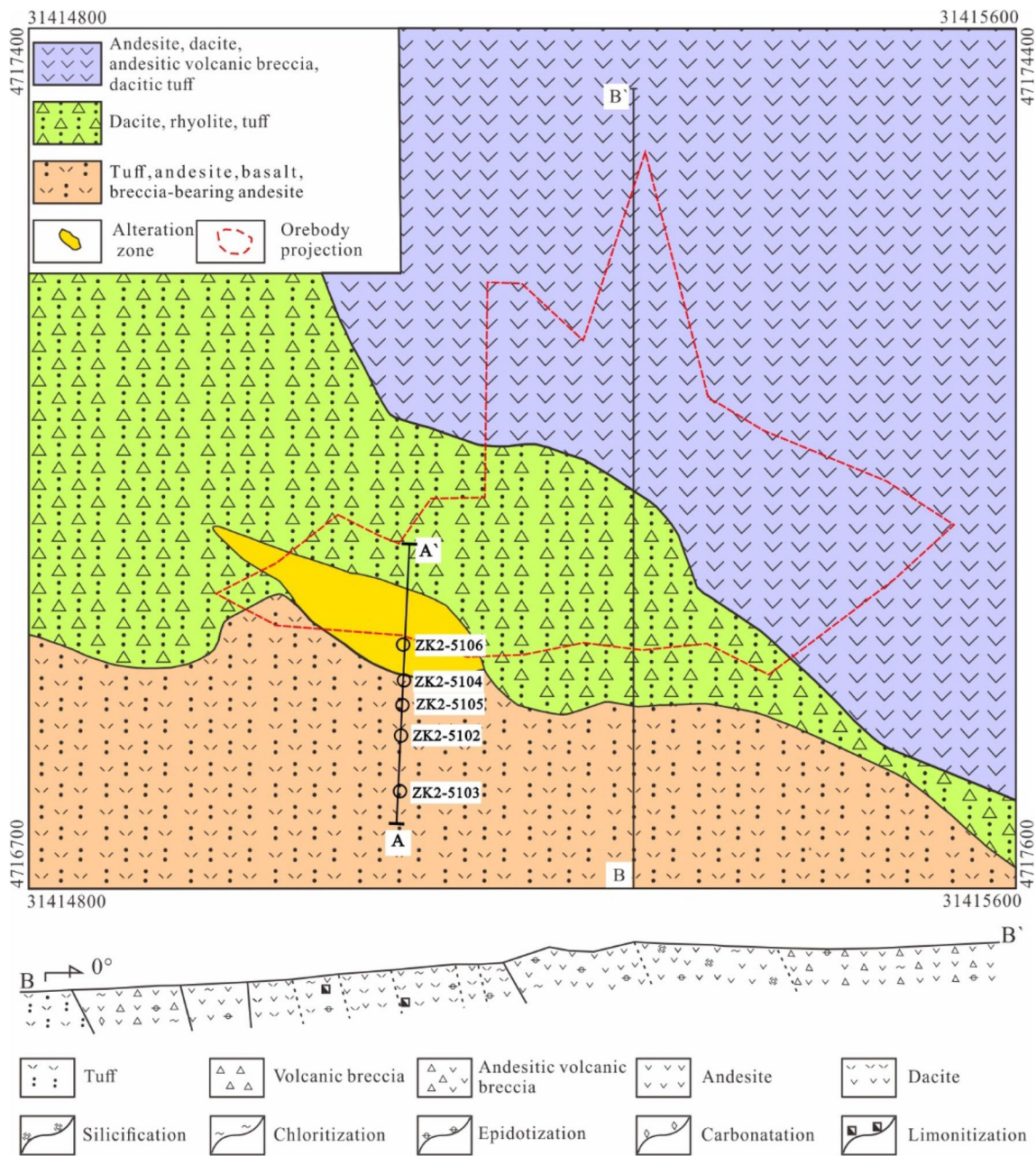


**Fig. 3** Geological sketch map of the Huangtan Au–Cu–Zn deposit (modified after XXMCL 2019)

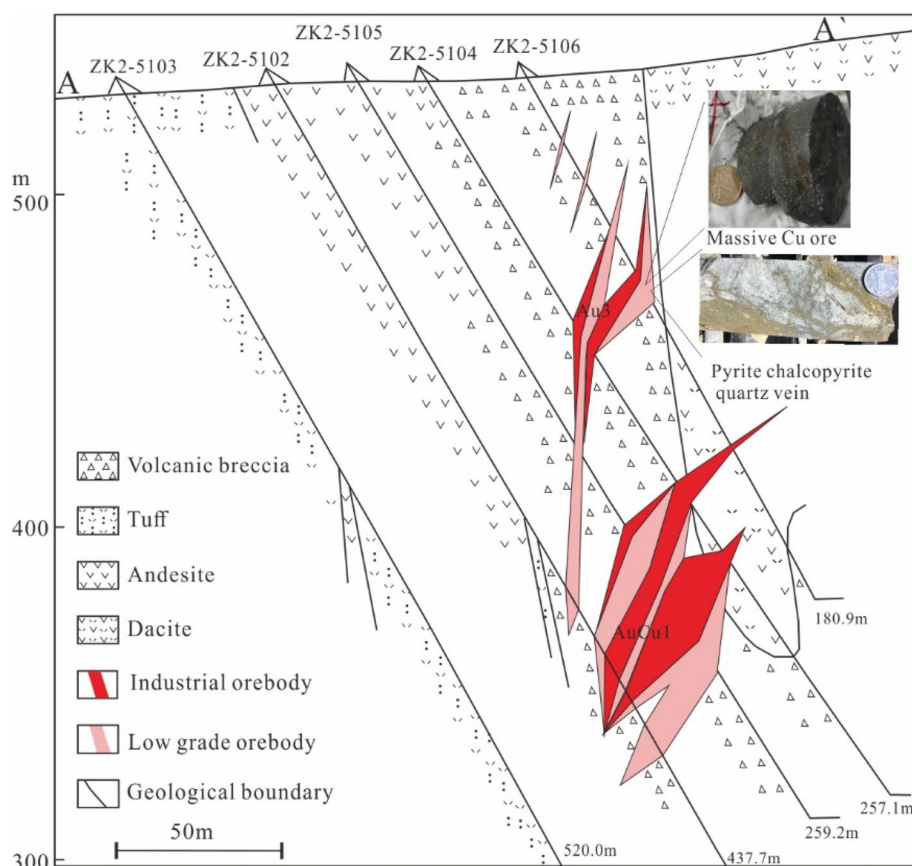
and chalcopyrite or fill fractures, cleavages or boundaries. “Invisible” gold is present in common pyrite, chalcopyrite, and tennantite. Nonmetallic minerals are quartz, sericite, chlorite, barite, and calcite.

The Huangtan Au–Cu–Zn deposit developed a series of hydrothermal alterations that are mainly distributed in and around the stockwork zones (Fig. 7A, B, F). Silicification, pyritization, and sericitization are the most important wall rock alterations. Pyrophyllitization is distributed in the cracks of the rock in the Huangtan deposit; and is related to structural activity after mineralization (Fig. 7C,

E). Propylitization is widely distributed in the Kalatag area (Fig. 7D), such as the Huangtan, Meiling (Yu 2014), Hongshi (Deng et al. 2014), and Honghai–Huangtupo ore districts (Huang et al. 2016).

Based on the mineral assemblages and cross-cutting relationships of the ore veins, the Huangtan Au–Cu–Zn deposit can be divided into three periods: exhalative–sedimentary, structure–hydrothermal and supergene periods (Fig. 8). The majority of mineralization occurred during the exhalative–sedimentary period, including strati-form mineralization of the exhalative–sedimentary units

**Fig. 4** Cross section of 5100 prospecting line of the Huangtan Au–Cu–Zn deposit (modified after XXMCL 2019)



and vein mineralization of the stockwork unit. Some of the sulfide in the orebody was compressed, deformed and broken, and no mineralization of industrial value developed during the structure–hydrothermal period. Limonite, malachite, covellite, sulfur, jarosite, and kaolinite formed during the supergene period (Fig. 7G, H, I).

## Sampling and analytical methods

### Sample description

Ore samples were collected from drill holes in the Huangtan Au–Cu–Zn deposit (vein mineralization, stratiform mineralization and altered wall rock: vein mineralization includes pyrite–chalcopyrite–sphalerite–telluride–gold–quartz veins in the stockwork unit; stratiform mineralization includes pyrite–chalcopyrite–sphalerite–galena–barite in the exhalative–sedimentary units; altered wall rock shows sericite–quartz–pyrite alteration in the stockwork unit). The vein, massive ore and altered wall rock represent the products of the main metallogenic period. The details are described in Table 1.

## Analytical methods

### Chalcopyrite Re–Os dating

Pure chalcopyrite grains were selected under a binocular microscope after the samples were crushed to 80–100 mesh. Chalcopyrite Re–Os isotope compositions were analyzed using a TJA X-series inductively coupled plasma mass spectrometer (ICP-MS) at the Re–Os laboratory of the National Research Center of Geoanalysis, Chinese Academy of Geological Sciences, Beijing. The detailed procedures of Re–Os chemical separation and ICP-MS measurement followed those described by Qu and Du (2003), Qu et al. (2009), Li et al. (2010) and Zhou et al. (2012). The measured masses for Re were 185 and 187; a mass of 190 was used to monitor Os. The measured masses for Os were 186, 187, 188, 189, 190 and 192; a mass 185 of was used to monitor Re. The average blanks for the total procedure were ~40 pg for Re, ~0.1 pg for Os and ~0.2 pg for  $^{187}\text{Os}$ . The reference material GBW04435 (JDC) was utilized to test the analytical reliability. The Re–Os isochron was calculated using the isoplot program (Ludwig 2003).



**Fig. 5** Photographs of representative ore samples from the Huangtan Au–Cu–Zn deposit. **A** Massive pyrite ores and disseminated pyrite ore; **B** Massive pyrite–chalcopyrite ores and pyrite–chalcopyrite vein; **C** Massive pyrite–chalcopyrite–sphalerite ores and pyrite–chalcopyrite vein; **D** Massive pyrite ores; **E** Massive pyrite–chalcopyrite ores;

**F** Massive pyrite–chalcopyrite–sphalerite ores; **G** Pyrite–chalcopyrite vein and silicification; **H** Pyrite–chalcopyrite vein; **I** Massive pyrite–barite ores; **J–L** Pyrite–chalcopyrite–quartz vein; **M** Altered wall rock. *Py* pyrite, *Ccp* chalcopyrite, *Sp* sphalerite, *Brt* barite, *Qtz* quartz

### Fluid inclusion analyses

Petrography and microthermometry of barite- and quartz-hosted fluid inclusion petrography and microthermometry were performed at the Fluid Inclusion Laboratory of Hefei University of Technology and China University of Geoscience, Beijing. Fluid inclusion types and assemblages were investigated by observation and identification under ZEISS Axioskop 40A and Nikon LV100 microscopes. Microthermometric data were gathered on a Linkam THMSG 600 programmable heating–freezing stage (–196 °C to +600 °C).

The estimated accuracies are  $\pm 0.1$  °C for temperatures lower than 30 °C,  $\pm 1$  °C for the interval of 31–300 °C, and  $\pm 2$  °C for the interval of 300–600 °C.

### Stable isotope analyses

The H–O, He–Ar and S isotope composition analyses were carried out at the MNR Key Laboratory of Metallogeny and Mineral Assessment, Institute of Mineral Resources, CAGS, Beijing.

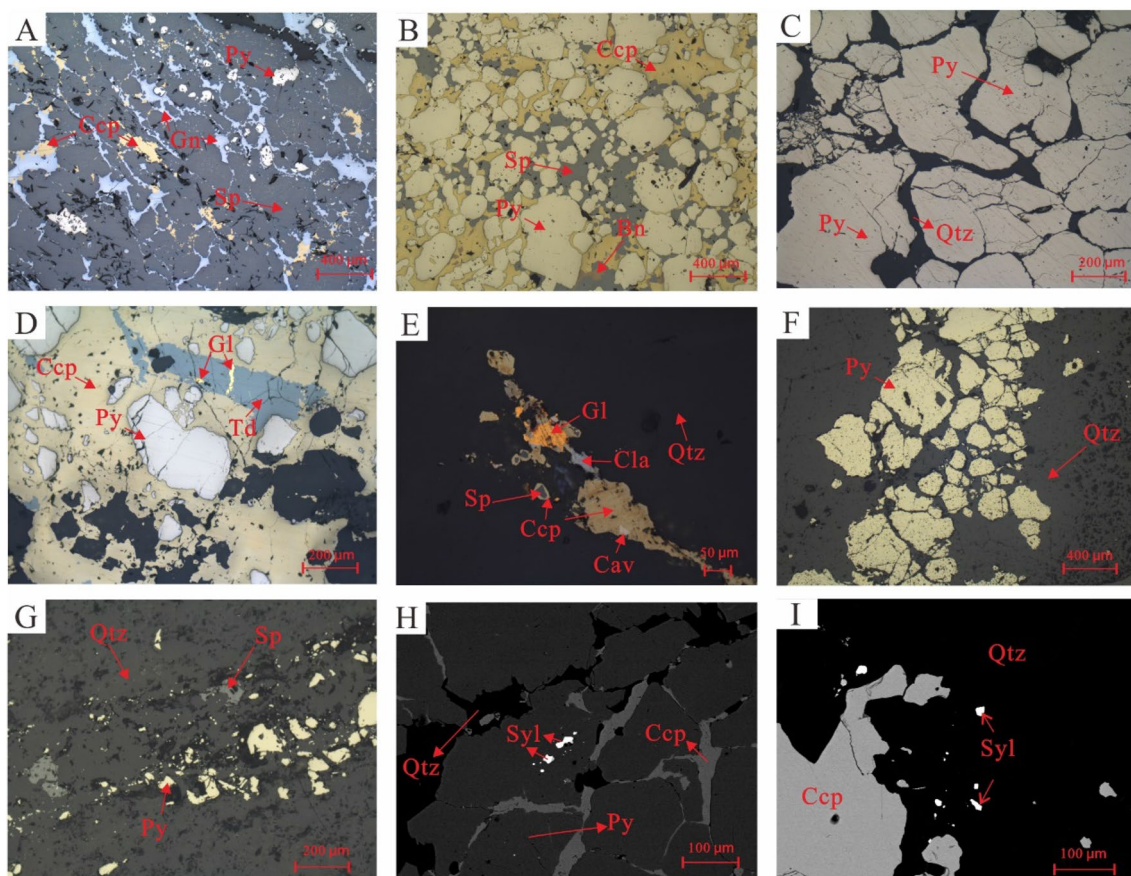


**Fig. 6** Photographs showing ore texture, structure and mineral assemblage of the Huangtan Au–Cu–Zn deposit: **A** massive ores of the contain sphalerite, galena, chalcopyrite and pyrite; **B** massive ores of the contain chalcopyrite, pyrite, sphalerite and bornite; **C** massive ores of the contain pyrite; **D** pyrite–chalcopyrite–gold vein of the contain chalcopyrite, pyrite, gold, tetrahedrite and gold have paragenetic relation with tetrahedrite; **E** pyrite–chalcopyrite–gold vein of the

contain chalcopyrite, pyrite, gold, calaverite, sphalerite, clausenthalite, quartz and gold included in chalcopyrite; **F** pyrite vein of the contain pyrite, quartz; **G** pyrite–sphalerite vein of the contain pyrite, sphalerite, quartz; **H, I** pyrite–chalcopyrite vein of the contain chalcopyrite, pyrite, sylvanite, quartz; *Py* pyrite, *Ccp* chalcopyrite, *Sp* sphalerite, *Gn* galena, *Cav* Calaverite, *Bn* bornite, *Syl* sylvanite, *Gl* gold, *Td* tetrahedrite, *Cl* clausenthalite, *Qtz* quartz

The hydrogen and oxygen isotope compositions of quartz were determined using a FinniganMAT253 mass spectrometer. Oxygen was extracted from quartz by the BrF<sub>5</sub> method (Clayton and Mayeda 1963), and the hydrogen isotope compositions of fluid inclusions were analyzed using the Zn reduction method (Coleman et al. 1982). The values of  $\delta^{18}\text{O}$  and  $\delta\text{D}$  are reported relative to the Vienna standard mean ocean water (V-SMOW), and the analytic precisions are  $\pm 0.2\text{‰}$  for  $\delta^{18}\text{O}$  and  $\pm 2\text{‰}$  for  $\delta\text{D}$ .

The He and Ar isotopes of the pyrite samples were measured with a Helix SFT instrument. The sensitivity of the Helix SFT for He was  $> 2 \times 10^{-4}$  amps/Torr at 800  $\mu\text{A}$ , and the sensitivity for was Ar  $> 1 \times 10^{-3}$  amps/Torr at 200  $\mu\text{A}$ . The resolution of Faraday is  $> 400$ , and the resolution of the multiplier is superior to 700, which could completely separate the  $^3\text{He}$

and  $^4\text{He}$ , HD+H<sub>3</sub> and  $^3\text{He}$ . The He and Ar analytical results are based on the atmosphere as a standard, with  $^3\text{He}/^4\text{He}$  of  $1.4 \times 10^{-6}$ , and  $^{40}\text{Ar}/^{36}\text{Ar}$  of 295.5. The detailed crushing and analytical procedures followed those described in Mao et al. (2002) and Xie et al. (2016).

The sulfur isotope compositions were determined using the SO<sub>2</sub> method of Robinson and Kusakabe (1975). For the sulfides, each sample was reacted with Cu<sub>2</sub>O powder to directly produce SO<sub>2</sub>. Sulfate minerals were purified to pure BaSO<sub>4</sub> by the carbonate–zinc oxide semi–melt method, and then SO<sub>2</sub> was prepared by the V<sub>2</sub>O<sub>5</sub> oxide and Cu<sub>2</sub>O method. The SO<sub>2</sub> gas was gathered and purified to analyse the sulfur isotope compositions using a Finnigan MAT253 mass spectrometer. The  $\delta^{34}\text{S}$  values are reported relative to Vienna Canon Diablo Troilite (V–CDT) sulfide and the analytical precision is  $\pm 0.2\text{‰}$ .



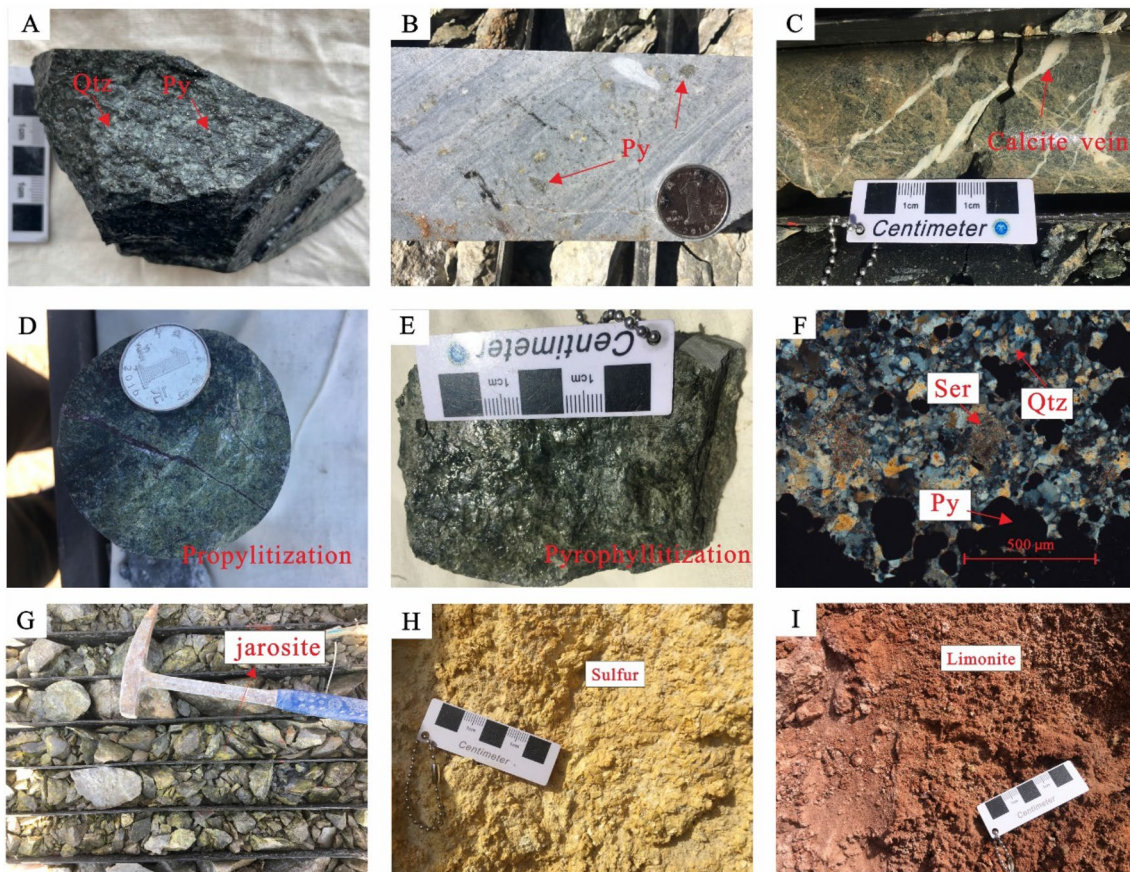


**Fig. 7** Representative photos the main alteration types from the Huangtan Au–Cu–Zn deposit: **A** pyritization, silicification in altered wall rock; **B** pyrite in tuff; **C** calcite veins in hanging wall; **D** propylitization in hanging wall; **E** pyrophyllitization distributed in the

cracks of the rock; **F** pyritization, silicification, sericitization in altered wall rock; **G** the jarosite distributed in the cracks of the rock; **H** the sulfur is distributed on the surface; **I** the limonite is distributed on the surface. *Py* pyrite, *Qtz* quartz, *Ser* sericite

## Analytical results

### Chalcopyrite Re–Os dating

The results of eight analyses of chalcopyrite from the Huangtan Au–Cu–Zn deposit are listed in Table 2. The tested chalcopyrite has 0.138 to 9.621 ppb Re and 0.437 to 44.868 ppt  $^{187}\text{Os}$ . Chalcopyrite samples contain common Os concentrations ranging from 0.389 to 15.363 ppt and  $^{187}\text{Re}/^{188}\text{Os}$  ratios between 122.5 and 14,618.6. The  $^{187}\text{Re}/^{188}\text{Os}$  vs.  $^{187}\text{Os}/^{188}\text{Os}$  isochron ages were calculated using the isoplot program (Ludwig 2003). Eight samples define an  $^{187}\text{Re}/^{188}\text{Os}$  vs.  $^{187}\text{Os}/^{188}\text{Os}$  isochron age of  $432 \pm 29$  Ma (mean square weighted deviation,  $\text{MSWD} = 28$ ) with an initial  $^{187}\text{Os}/^{188}\text{Os}$  ratio of  $0.9 \pm 2.4$  (Fig. 9). Four out of eight samples yield an isochron age of  $430 \pm 15$  Ma ( $\text{MSWD} = 0.53$ ), with initial  $^{187}\text{Os}/^{188}\text{Os}$  ratios of  $0.55 \pm 0.94$ .

### Fluid inclusions

Twenty-seven samples from the exhalative–sedimentary units and stockwork unit were measured, although primary inclusions were analyzed here, as defined by the textural criteria of Roedder (1984). The microthermometric data are summarized in Table 3. Primary inclusions are generally distributed along growth zones, in isolation or in random clusters within intragranular crystals (Roedder 1984). The fluid inclusions in quartz and barite from the Huangtan Au–Cu–Zn deposit are predominantly liquid-rich two-phase inclusions (L-type) (Fig. 10C, D, E, G, H, I), pure liquid inclusions (P-type) (Fig. 10A, B), and rare vapor-rich two-phase inclusions (V-type) (Fig. 10F). The lengths of these inclusions are generally 1–12  $\mu\text{m}$ , and the inclusions have ellipsoidal, irregular, linear, and negative crystal shapes. The liquid-rich inclusions contain vapor bubbles ranging from 3 to 50 vol%, and the vapor-rich

**Table 1** List of samples collected for the study from the Huangtan Au–Cu–Zn deposit

Sample number	Drillhole depth (m)	Rock types	Mineral assemblage	Mineral				Fluid inclusion
				Re–Os	He–Ar	H–O	S	
ZK1201-19-5	Drillhole 1201, 336	Altered wall rock	Qtz + Py + Ser					Qtz
ZK1201-19-6	Drillhole 1201, 340	Altered wall rock	Qtz + Py + Ser					Qtz
ZK1401-19-3	Drillhole 1401, 259	Altered wall rock	Qtz + Py + Ser					Qtz
ZK2-5205-B1	Drillhole 5205, 323	Stratiform mineralization	Br + Py			Br	Br	Br
ZK5102-19-13	Drillhole 5102, 223	Vein mineralization	Py + Ccp + Qtz					Qtz
ZK5102-19-4	Drillhole 5102, 214	Altered wall rock	Qtz + Py + Ser					Qtz
ZK5105-19-2	Drillhole 5105, 137	Vein mineralization	Py + Ccp + Qtz					Qtz
ZK5105-19-4	Drillhole 5105, 158	Vein mineralization	Py + Ccp + Qtz					Qtz
ZK5105-19-9	Drillhole 5105, 174	Vein mineralization	Py + Ccp + Qtz					Qtz
ZK5106-19-5	Drillhole 5106, 76	Vein mineralization	Py + Ccp + Qtz					Qtz
ZK5154-18-10	Drillhole 5154, 163	Vein mineralization	Py + Ccp + Te + Qtz	Ccp				Qtz
ZK5154-18-11	Drillhole 5154, 188	Vein mineralization	Py + Ccp + Qtz + Sp	Ccp				Qtz
ZK5154-18-12	Drillhole 5154, 203	Vein mineralization	Py + Ccp + Qtz		Py		Py	Qtz
ZK5154-18-13	Drillhole 5154, 206	Vein mineralization	Py + Ccp + Qtz				Py	Qtz
ZK5154-18-14	Drillhole 5154, 203	Vein mineralization	Py + Ccp + Qtz				Py	Qtz
ZK5154-18-15	Drillhole 5154, 215	Vein mineralization	Py + Ccp + Qtz			Qtz	Py	Qtz
ZK5154-18-16	Drillhole 5154, 226	Stratiform mineralization	Py + Ccp + Qtz + Sp		Py		Py	Qtz
ZK5154-18-17	Drillhole 5154, 102	Vein mineralization	Py + Ccp + Qtz					Qtz
ZK5154-18-2	Drillhole 5154, 157	Vein mineralization	Py + Ccp + Te + Qtz				Py, Ccp	
ZK5154-18-3	Drillhole 5154, 153	Vein mineralization	Py + Ccp + Te + Qtz	Ccp			Py, Ccp	
ZK5154-18-4	Drillhole 5154, 155	Vein mineralization	Py + Ccp + Te + Qtz	Ccp			Py, Ccp	
ZK5154-18-5	Drillhole 5154, 156	Vein mineralization	Py + Ccp + Te + Qtz + Sp	Ccp			Py, Ccp	
ZK5154-18-6	Drillhole 5154, 155	Vein mineralization	Py + Ccp + Te + Qtz	Ccp		Qtz	Py, Ccp	Qtz
ZK5154-18-7	Drillhole 5154, 163	Vein mineralization	Py + Ccp + Te + Qtz					Qtz
ZK5154-18-8	Drillhole 5154, 173	Vein mineralization	Py + Ccp + Te + Qtz	Ccp	Py		Py, Ccp	
ZK5154-18-9	Drillhole 5154, 155	Vein mineralization	Py + Ccp + Te + Qtz	Ccp		Qtz		Qtz
ZK5203-18-6	Drillhole 5203, 301	Stratiform mineralization	Br + Py			Br	Br	Br
ZK5203-18-7	Drillhole 5203, 300	Stratiform mineralization	Br + Py			Br	Br	Br
TG17-10	Drillhole 5302	Altered wall rock	Qtz + Py + Ser				Py	
TG17-11	Drillhole 5302	Altered wall rock	Qtz + Py + Ser				Py, Ccp	
TG17-2	Drillhole 5302	Altered wall rock	Qtz + Py + Ser				Py	Qtz
TG17-3	Drillhole 5302	Altered wall rock	Qtz + Py + Ser			Qtz	Py	Qtz
TG17-4	Drillhole 5302	Altered wall rock	Qtz + Py + Ser			Qtz	Py	Qtz
TG17-5	Drillhole 5302	Altered wall rock	Qtz + Py + Ser				Py	
TG17-6	Drillhole 5302	Altered wall rock	Qtz + Py + Ser				Py	
TG17-7	Drillhole 5302	Altered wall rock	Qtz + Py + Ser			Qtz	Py	Qtz
TG17-8	Drillhole 5302	Altered wall rock	Qtz + Py + Ser			Qtz	Py	Qtz
TG17-9	Drillhole 5302	Altered wall rock	Qtz + Py + Ser			Qtz	Py	Qtz

Ccp chalcopyrite, Py pyrite, Qtz quartz, Sp sphalerite, Ser sericite, Br barite, Te telluride

two-phase inclusions contain vapor bubbles ranging from 50 to 80 vol%.

The fluid inclusions in quartz from the altered wall rock samples are predominantly L-type, P-type, and rare V-type fluid inclusions. The L-type fluid inclusions homogenize to liquid at 120–352 °C, and their ice-melting temperatures vary from –7.1 to –1.4 °C, which correspond to calculated salinities of 2.4–10.6 wt% NaCl equiv (Bodnar 1993), and

densities ranging from 0.68 to 0.97 g/cm<sup>3</sup>. The V-type fluid inclusions homogenize to vapor at 273–318 °C.

The fluid inclusions in quartz from vein mineralization are predominantly L-type, P-type, and rare V-type fluid inclusions. The L-type fluid inclusions homogenize to liquid at 116–340 °C, and their ice-melting temperatures vary from –9.6 to –0.6 °C, which correspond to calculated salinities of 1.1–13.5 wt% NaCl equiv., and densities

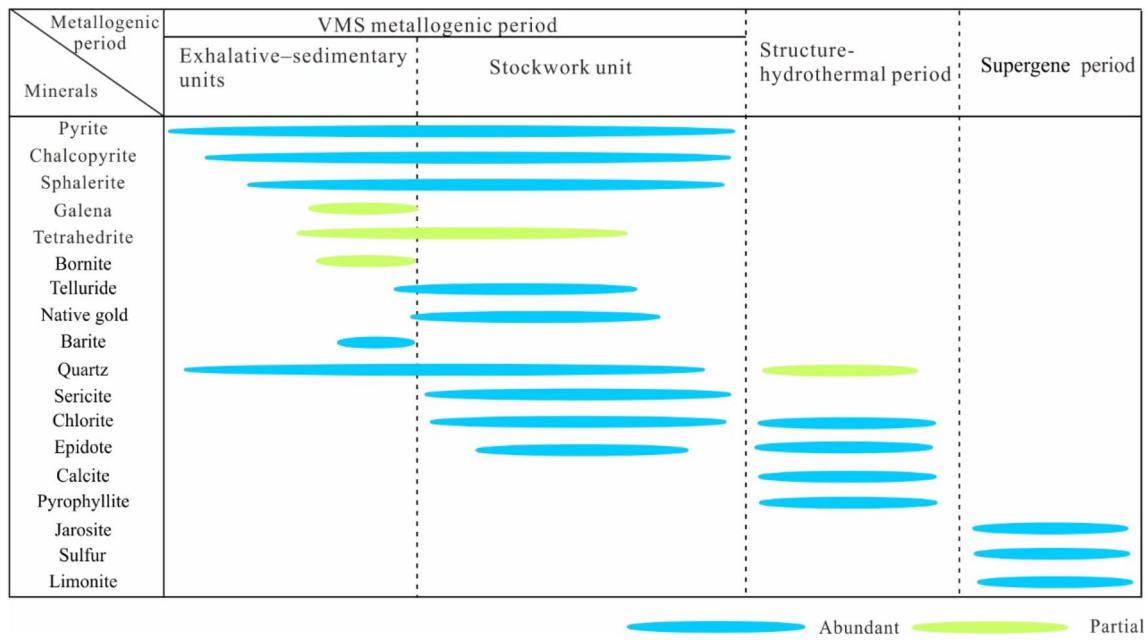


Fig. 8 Mineral paragenesis for the Huangtan Au–Cu–Zn deposit

Table 2 Re–Os isotopic data for chalcopyrite from the Huangtan Au–Cu–Zn deposit

Sample no.	Remarks	Weight	Re(ppb)	Common Os (ppt)	<sup>187</sup> Os (ppt)	<sup>187</sup> Re/ <sup>188</sup> Os	<sup>187</sup> Os/ <sup>188</sup> Os
ZK5154-18-3	Vein mineralization	0.30034	0.138 ± 0.001	5.485 ± 0.08	0.437 ± 0.004	122.5 ± 1.9	0.62 ± 0.01
ZK5154-18-4	Vein mineralization	0.30016	0.504 ± 0.004	2.377 ± 0.05	3.449 ± 0.08	931.1 ± 22.8	9.28 ± 0.18
ZK5154-18-5	Vein mineralization	0.30026	0.333 ± 0.003	2.264 ± 0.05	1.233 ± 0.01	710.2 ± 15.1	4.21 ± 0.08
ZK5154-18-6	Vein mineralization	0.65028	1.254 ± 0.009	0.414 ± 0.01	5.692 ± 0.04	14,618.6 ± 203.9	105.75 ± 1.18
ZK5154-18-8	Vein mineralization	0.65011	9.621 ± 0.071	15.363 ± 0.12	44.868 ± 0.34	3025 ± 31	22.44 ± 0.05
ZK5154-18-9	Vein mineralization	0.65035	1.847 ± 0.014	1.601 ± 0.01	8.455 ± 0.06	5572.4 ± 60.2	40.60 ± 0.18
ZK5154-18-10	Vein mineralization	0.65088	0.257 ± 0.002	0.389 ± 0.003	1.175 ± 0.01	3193.2 ± 35.2	23.09 ± 0.1
ZK5154-18-11	Vein mineralization	0.65034	1.706 ± 0.013	2.258 ± 0.06	9.213 ± 0.09	3648 ± 109.9	31.5 ± 0.76

ranging from 0.72 to 1.01 g/cm<sup>3</sup>. The V-type fluid inclusions homogenize to vapor at 336–338 °C.

L-type inclusions developed in sphalerite from exhalative–sedimentary units. Since the temperature measurement conditions were not met, no microthermometry measurements were performed. The fluid inclusions in barite from the exhalative–sedimentary units are predominantly L-type, P-type, and rare V-type fluid inclusions. The L-type fluid inclusions homogenize to liquid at 123–369 °C, and their ice-melting temperatures vary from –5.3 to –2.2 °C, thus corresponding to calculated salinities of 3.7–8.3 wt% NaCl equiv., and densities ranging from 0.62 to 0.83 g/cm<sup>3</sup>. The V-type fluid inclusions homogenize to vapor at 341 °C, and their ice-melting temperature is –4.5 °C, corresponding to calculated salinity of 7.2 wt% NaCl equiv.

### H and O stable isotopes

The analytical results of eleven H and O stable isotope analyses of quartz and barite from the Huangtan Au–Cu–Zn deposit are presented in Table 4. The δ<sup>18</sup>D<sub>V-SMOW</sub> values of fluids in quartz from the altered wall rock range from –69 to –42‰ with a mean of –54‰. The δ<sup>18</sup>O<sub>V-SMOW</sub> values of quartz from the altered wall rock range from 8.0 to 10.1‰, with a mean of 9.1‰. Using the quartz–water fractionation equation 1000lnα = 3.38 × 10<sup>6</sup> T<sup>–2</sup> – 3.40 (Clayton et al. 1972) and the average homogenization temperature of fluid inclusions in quartz in the same sample, the calculated δ<sup>18</sup>O<sub>fluid</sub> values of the fluids are –7.24 to –1.07‰.

The δ<sup>18</sup>D<sub>V-SMOW</sub> values of fluids in quartz from vein mineralization range from –69 to –58‰ with a mean of –62‰. The δ<sup>18</sup>O<sub>V-SMOW</sub> values of quartz from vein

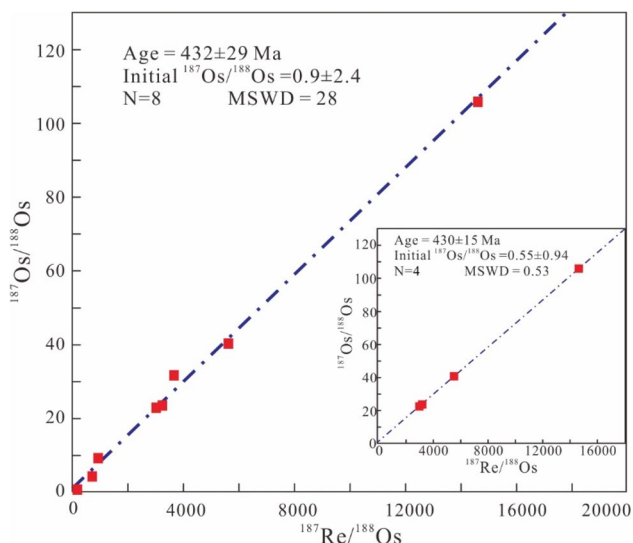


**Fig. 9**  $^{187}\text{Re}/^{188}\text{Os}$  vs.  $^{187}\text{Os}/^{188}\text{Os}$  isochron diagram for chalcopyrite from the Huangtan Au–Cu–Zn deposit

mineralization range from 8.6 to 9.3‰, with a mean of 8.8‰, and the calculated  $\delta^{18}\text{O}_{\text{fluid}}$  values of the fluids are  $-7.14$  to  $-0.01$ ‰.

The  $\delta D_{\text{V-SMOW}}$  values of fluids in barite from the exhalative–sedimentary units vary from  $-66$  to  $-52$ ‰, with a mean of  $-59$ ‰. The  $\delta^{18}\text{O}_{\text{V-SMOW}}$  values of barite range from 7.4‰ to 7.8‰, with a mean of 7.6‰. Using the barite–water fractionation equation  $1000 \ln \alpha = 3.01 \times 10^6 T^{-2} - 7.30$  (Kusakabe and Robinson 1977) and the average homogenization temperature of fluid inclusions in barite in the same sample, the calculated  $\delta^{18}\text{O}_{\text{fluid}}$  values of the fluids are 0.16 to 6.81‰.

### He and Ar isotopes

The He and Ar isotope compositions of fluid inclusions in pyrite from the Huangtan Au–Cu–Zn deposit are shown in Table 5. The  $^4\text{He}$  values of fluids in pyrite from vein mineralization are  $6.93 \times 10^{-8}$  and  $4.39 \times 10^{-8}$ , the  $^3\text{He}$  values are  $133.43 \times 10^{-8}$  and  $57.02 \times 10^{-8}$  ( $\text{cm}^3\text{STP/g}$ ), and the normalized  $^3\text{He}/^4\text{He}$  ratios are 0.929–1.374 (R/Ra). The  $^4\text{He}$  and  $^3\text{He}$  values of fluids in pyrite from massive ore in the exhalative–sedimentary units are  $12.78 \times 10^{-8}$  and  $219.29 \times 10^{-8}$  ( $\text{cm}^3\text{STP/g}$ ), respectively, and the  $^3\text{He}/^4\text{He}$  ratio is 1.226 (R/Ra). The  $^{40}\text{Ar}$  values of fluids in pyrite from vein mineralization range from  $3.67 \times 10^{-8}$  to  $8.02 \times 10^{-8}$  ( $\text{cm}^3\text{STP/g}$ ), and the value for pyrite from massive ore is  $4.54 \times 10^{-8}$  ( $\text{cm}^3\text{STP/g}$ ). The  $^{40}\text{Ar}/^{36}\text{Ar}$  ratios of vein mineralization are 388–459, and the ratios of massive ore are 502. The  $^{40}\text{Ar}/^4\text{He}$  ratios of vein mineralization are 0.836–1.157 those of massive ore are 0.355.

**Table 3** Microthermometric data for the different types of the fluid inclusions from the Huangtan Au–Cu–Zn deposit

Remarks	Description	Mineral	FI types	Size ( $\mu\text{m}$ )	Vapor (%)	Th, total $^{\circ}\text{C}$	Tm, ice $^{\circ}\text{C}$		$\rho$ ( $\text{g}/\text{cm}^3$ )
							Range (n)	Peak value	
Exhalative–sedimentary unit	Stratiform mineralization	Barite	L	2–10	3–20	123–369 (14)	–5.3 to –2.2	3.7–8.3(4)	0.62–0.83
		Barite	V	4–8	60	341 (1)	–4.5	7.2	0.72
Stockwork unit	Altered wall rock	Quartz	L	1–12	3–50	120–352 (94)	–7.1 to –1.4	2.4–10.6(53)	0.68–0.97
		Quartz	V	2–8	50–80	273–318 (2)	–	–	–
	Vein mineralization	Quartz	L	1–10	3–50	116–340 (130)	–9.6 to –0.6	1.1–13.5(71)	0.72–1.01
		Quartz	V	2–5	60–80	336–338(2)	–	–	–

Th, total  $^{\circ}\text{C}$ —total homogenization temperature; Tm, ice  $^{\circ}\text{C}$ —melting temperature of ice; (n)—the number of inclusions

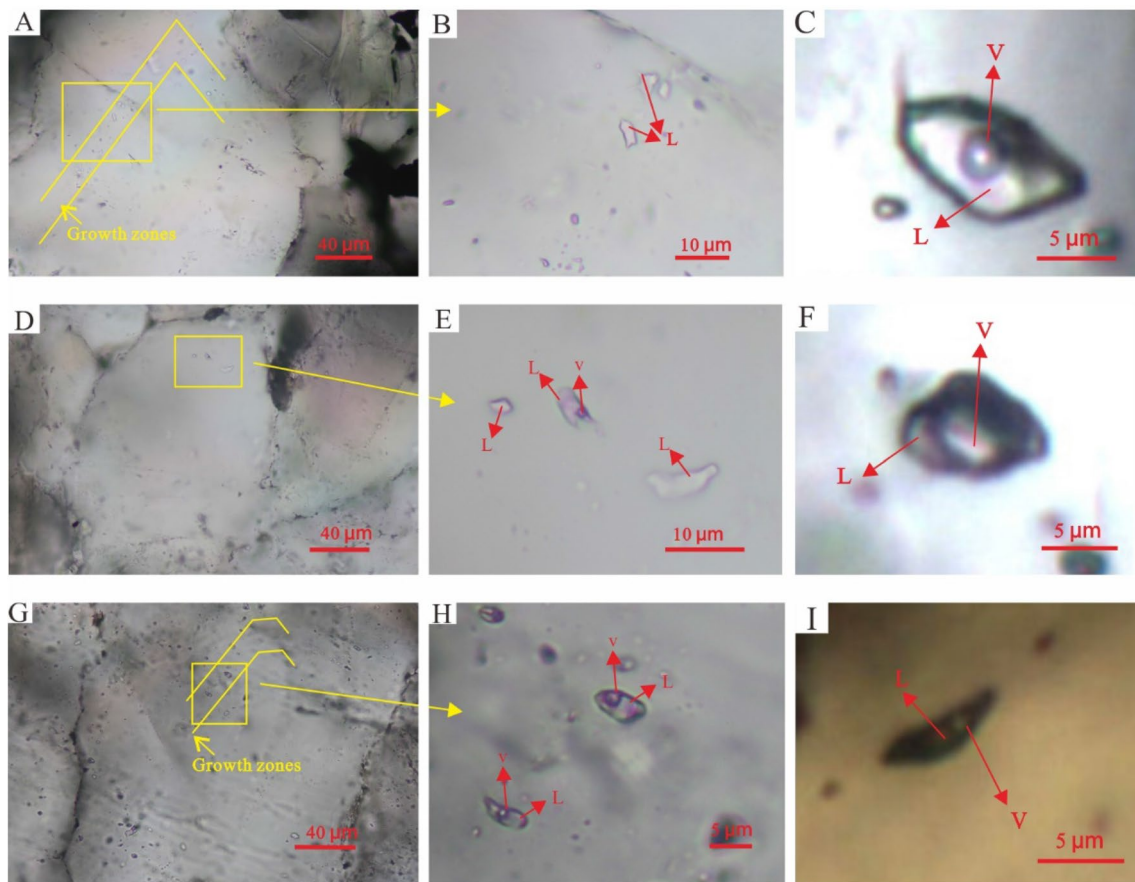


**Fig. 10** Photomicrographs of fluid inclusions from the Huangtan Au–Cu–Zn deposit: **A, B** pure liquid inclusion in quartz; **C** liquid inclusion in barite. **D, E, G, H** pure liquid and liquid inclusion in quartz; **F** vapor-rich inclusions in barite; **I** liquid inclusion in sphalerite

**Table 4** Oxygen and hydrogen isotopes of quartz and barite from the Huangtan Au–Cu–Zn deposit

No	Sample	Remarks	Mineral	$\delta^{18}\text{O}_{\text{V-SMOW}}$ (‰)	$\delta^{18}\text{O}_{\text{fluid}}$ (‰)	$\delta^{18}\text{D}_{\text{V-SMOW}}$ (‰)	Th (°C)
1	TG17-3	Altered wall rock	Quartz	9.1	−5.37	−54	162
2	TG17-4	Altered wall rock	Quartz	10.1	−7.24	−69	131
3	TG17-7	Altered wall rock	Quartz	9.0	−1.42	−42	221
4	TG17-8	Altered wall rock	Quartz	9.3	−1.07	−48	222
5	TG17-9	Altered wall rock	Quartz	8.0	−5.25	−55	177
6	ZK5154-18-6	Vein mineralization	Quartz	8.6	−3.85	−69	189
7	ZK5154-18-9	Vein mineralization	Quartz	9.3	−7.14	−58	140
8	ZK5154-18-15	Vein mineralization	Quartz	8.6	−0.01	−59	257
9	ZK5203-18-6	Stratiform mineralization	Barite	7.6	1.08	−52	194
10	ZK5203-18-7	Stratiform mineralization	Barite	7.8	6.81	−66	330
11	ZK2-5205-B1	Stratiform mineralization	Barite	7.4	0.16	−60	182

### Sulfur isotope analysis

The sulfur isotope compositions in pyrite and barite from the Huangtan Au–Cu–Zn deposit are shown in Table 6. The  $\delta^{34}\text{S}_{\text{V-CDT}}$  values of pyrite from the altered wall rock range

from −2.0 to 1.5‰, and the  $\delta^{34}\text{S}_{\text{V-CDT}}$  value of chalcopyrite is 0.2‰. The  $\delta^{34}\text{S}_{\text{V-CDT}}$  values of pyrite from vein mineralization range from −0.4 to 0.9‰, and the  $\delta^{34}\text{S}_{\text{V-CDT}}$  values of chalcopyrite range from −1.0 to −0.1‰. The  $\delta^{34}\text{S}_{\text{V-CDT}}$  values of barite from the exhalative–sedimentary units range

**Table 5** Helium and argon isotopic compositions of fluid inclusions in pyrite from the Huangtan Au–Cu–Zn deposit

	ZK5154-18-8	ZK5154-18-12	ZK5154-18-16
Samples	Vein mineralization	Vein mineralization	Stratiform mineralization
$^4\text{He} \times 10^{-8} (\text{cm}^3 \text{STP/g})$	6.93	4.39	12.78
$^3\text{He} \times 10^{-15} (\text{cm}^3 \text{STP/g})$	133.43	57.02	219.29
$^3\text{He}/^4\text{He} (\times 10^{-7})$	$19.24 \pm 2.97$	$13 \pm 1.62$	$17.16 \pm 2.21$
$^3\text{He}/^4\text{He} (\text{R/Ra})$	$1.374 \pm 0.21$	$0.929 \pm 0.12$	$1.226 \pm 0.16$
$\text{He}^{\text{M}} (\%)$	20.90	14.02	18.61
$^{40}\text{Ar} \times 10^{-8} (\text{cm}^3 \text{STP/g})$	8.02	3.67	4.54
$^{40}\text{Ar}/^{36}\text{Ar}$	$459.2 \pm 1.39$	$388 \pm 1.14$	$502 \pm 2.74$
$^{40}\text{Ar}/^4\text{He}$	1.157	0.836	0.355
$^{40}\text{Ar}^* (\%)$	35.65	23.83	41.13
$^{40}\text{Ar}^*/^4\text{He}$	0.412	0.199	0.146
$\text{F}^4\text{He}$	2405	2813	8570

$\text{He}^{\text{M}}$  is the mantle cause helium isotopes;  $^{40}\text{Ar}^*$  is the radioactive  $^{40}\text{Ar}$  isotopes; R is  $^3\text{He}/^4\text{He}$  ratio of the sample; Calculations using parameter is internationally recognized as the earth's atmosphere:  $^4\text{He}/^{40}\text{Ar} = 0.00056328$ ,  $\text{Ra} = ^3\text{He}/^4\text{He} = 1.4 \times 10^{-6}$ ,  $^{40}\text{Ar}/^{36}\text{Ar} = 295.5$ .  $^{40}\text{Ar} = [1 - [295.5 / (^{40}\text{Ar}/^{36}\text{Ar})]] \times 100 (\%)$ .  $\text{He}^{\text{M}} (\%) = 100 \times (\text{R} - \text{R}_c) / (\text{R}_m - \text{R}_c)$ , where  $\text{R}_m = 6.5$  and  $\text{R}_c = 0.02$  represent the  $^3\text{He}/^4\text{He}$  ratios of the fluids in the mantle and crust

**Table 6**  $\delta^{34}\text{S}_{\text{V-CDT}}$  values of sulfide and barite samples from the Huangtan Au–Cu–Zn deposit

No.	Sample no.	Remarks	Mineral	$\delta^{34}\text{S}_{\text{V-CDT}} (\%)$	No.	Sample no.	Remarks	Mineral	$\delta^{34}\text{S}_{\text{V-CDT}} (\%)$
1	ZK5203-18-6	Stratiform mineralization	Barite	24.7	17	ZK5154-18-5-1	Vein mineralization	Pyrite	-0.5
2	ZK5203-18-7	Stratiform mineralization	Barite	24.8	18	ZK5154-18-6-1	Vein mineralization	Pyrite	0.3
3	ZK2-5205-B1	Stratiform mineralization	Barite	24.1	19	ZK5154-18-8-1	Vein mineralization	Pyrite	-0.4
4	TG17-3	Altered wall rock	Pyrite	0.6	20	ZK5154-18-13	Vein mineralization	Pyrite	0.9
5	TG17-4	Altered wall rock	Pyrite	0.4	21	ZK5154-18-14	Vein mineralization	Pyrite	0.5
6	TG17-7	Altered wall rock	Pyrite	0.2	22	ZK5154-18-15	Vein mineralization	Pyrite	0.5
7	TG17-8	Altered wall rock	Pyrite	0.3	23	ZK5154-18-12	Vein mineralization	Pyrite	0.8
8	TG17-9	Altered wall rock	Pyrite	1.0	24	ZK5154-18-16	Stratiform mineralization	Pyrite	0.4
9	TG17-2	Altered wall rock	Pyrite	-1.2	25	ZK5154-18-2	Vein mineralization	Chalcopyrite	-0.8
10	TG17-5	Altered wall rock	Pyrite	0.8	26	ZK5154-18-3	Vein mineralization	Chalcopyrite	-0.7
11	TG17-6	Altered wall rock	Pyrite	1.0	27	ZK5154-18-4	Vein mineralization	Chalcopyrite	-0.8
12	TG17-10	Altered wall rock	Pyrite	-2.0	28	ZK5154-18-5	Vein mineralization	Chalcopyrite	-0.9
13	TG17-11-1	Altered wall rock	Pyrite	1.5	29	ZK5154-18-6	Vein mineralization	Chalcopyrite	-0.1
14	ZK5154-18-2-1	Vein mineralization	Pyrite	-0.3	30	ZK5154-18-8	Vein mineralization	Chalcopyrite	-1.0
15	ZK5154-18-3-1	Vein mineralization	Pyrite	0.2	31	TG17-11-2	Altered wall rock	Chalcopyrite	0.2
16	ZK5154-18-4-1	Vein mineralization	Pyrite	-0.3					

from 24.1 to 24.7‰, and the  $\delta^{34}\text{S}_{\text{V-CDT}}$  value of pyrite is 0.4‰.

## Discussion

### Time of mineralization

The volcanic rocks of the Ordovician–Silurian Daliugou (Unit 1), Silurian Hongliuxia (Unit 2) and Kalatag (Unit 3) formations formed at > 446 to 416 Ma (Table 7). Among these, the U–Pb ages of tuff, sedimentary tuff, andesitic tuff and dacitic tuff in Unit 2 are  $423.3 \pm 2.9$  Ma,  $440.4 \pm 2.9$  Ma,  $442.0 \pm 1.1$  Ma, and  $438 \pm 5$  Ma, respectively (Xu 2017; Chai et al. 2019; Cheng et al. 2020a; Sun et al. 2020), indicating that tuffs were formed in the Early Silurian (423–442 Ma). The Huangtan deposit has the characteristics of VMS-type mineralization, in which the layered orebody of the Huangtan deposit is strata bounded by Unit 2, and the ore-forming

age of the layered orebody is roughly the same as that of volcanic rocks (the host-rocks of the orebodies include tuff and volcanic breccia). Therefore, the approximate Huangtan mineralization age should be Early Silurian.

The Re–Os radiogenic system in chalcopyrite can be utilized as a high-precision geochronometer, and this dating method has the advantage of an isotopic closure temperature of > 500 °C (Nozaki et al. 2010), meaning that the results are not easily disturbed by subsequent metamorphism or deformation. Therefore, chalcopyrite is likely to record the timing of primary crystallization. The Re–Os ratios of chalcopyrite are different from those of molybdenite. Molybdenite contains little Os, so the data are not easy to extrapolate, and the obtained MSWD values are often very small. Chalcopyrite and pyrite contain normal amounts of Os and a normal initial  $^{187}\text{Os}/^{188}\text{Os}$  ratio. Therefore, the Re–Os isochron ages of chalcopyrite and pyrite are relatively variable. However, small variations in the initial Os of the samples do not prevent the reliable calculation of a

**Table 7** Summary of geochronological data for ore deposits and volcanic rocks from the Kalatag district

Deposits	Type	Dating samples	Mineral	Dating methods	Age (Ma)	References
Honghai	VMS	Massive ore	Chalcopyrite	Re–Os isochron	$434.2 \pm 3.9$	Deng et al. (2016)
		Phyllic alteration zone	Sericite	Ar–Ar plateau	$438.8 \pm 3.0$	Deng et al. (2018b)
				Ar–Ar isochron	$443 \pm 11$	Deng et al. (2018b)
Huangtupo	VMS	Massive ore	Pyrite	Re–Os isochron	$436.1 \pm 2.3$	Mao et al. (2019)
		Massive ore	Pyrite, chalcopyrite, sphalerite	Rb–Sr isochron	$432.2 \pm 3.1$	Yang et al. (2018a)
				Re–Os isochron	$425 \pm 38$	Yang et al. (2018a)
Huangtan	VMS	Massive ore	Chalcopyrite	Re–Os isochron	$429.5 \pm 10$	Cheng et al. (2020a)
		Vein ore	Chalcopyrite	Re–Os isochron	$432 \pm 29$	This study
				Pyrite	Re–Os isochron	$437.9 \pm 6.6$
Hongshi	Vein	Quartz vein ore	Chalcopyrite	Re–Os isochron	$431.8 \pm 2.7$	Deng et al. (2016)
		Phyllic alteration zone	Sericite	Ar–Ar plateau	$441.5 \pm 3.2$	Deng et al. (2018b)
				Ar–Ar isochron	$445.8 \pm 5.6$	Deng et al. (2018b)
				Ar–Ar plateau	$446.4 \pm 4.6$	Deng et al. (2018b)
Volcanic rocks		Dacite	Zircon	LA–ICP–MS U–Pb	$438.4 \pm 4.9$	Li et al. (2016)
		Andesite	Zircon	LA–ICP–MS U–Pb	$434.8 \pm 3.8$	Li et al. (2016)
		Dacite	Zircon	LA–ICP–MS U–Pb	$440.1 \pm 1.2$	Chai et al. (2019)
		Andesite	Zircon	LA–ICP–MS U–Pb	$439.7 \pm 0.95$	Chai et al. (2019)
		Andesitic tuff	Zircon	LA–ICP–MS U–Pb	$442.0 \pm 1.1$	Chai et al. (2019)
		Felsic volcanic rocks	Zircon	SIMS U–Pb	$416.3 \pm 5.9$	Mao et al. (2010)
		Sericitized rocks	Sericite	K–Ar age	$424 \pm 7$	Mao et al. (2010)
		Basaltic andesite	Zircon	LA–ICP–MS U–Pb	$427 \pm 2.1$	Yu (2014)
		Dacite	Zircon	SIMS U–Pb	$441.4 \pm 2.6$	Xu (2017)
		Sedimentary tuff	Zircon	SIMS U–Pb	$440.4 \pm 2.9$	Xu (2017)
		Rhyolitic volcanic Breccia lava	Zircon	SHRIMP U–Pb	$439.9 \pm 4.8$	Long et al. (2017)
		Rhyolite	Zircon	SHRIMP U–Pb	$439 \pm 7$	Long et al. (2017)
		Tuff	Zircon	LA–ICP–MS U–Pb	$423.3 \pm 2.9$	Cheng et al. (2020a)
		Dacitic tuff	Zircon	LA–ICP–MS U–Pb	$438 \pm 5$	Sun et al. (2020)

Re–Os isochron age (Stein and Hannah 2014). The Re–Os geochronology of chalcopyrite has been applied in different types of hydrothermal systems (Han et al. 2007, 2010; Lawley et al. 2013; Ye et al. 2013; Zhu and Sun 2013; Ying et al. 2014; Deng et al. 2016). The vein mineralization age of the Huangtan Au–Cu–Zn deposit can be obtained by directly dating the primary ore chalcopyrite. We obtained a  $^{187}\text{Re}/^{188}\text{Os}$  vs.  $^{187}\text{Os}/^{188}\text{Os}$  isochron age for 8 chalcopyrite samples of  $432 \pm 29$  Ma (MSWD = 28). Due to the large uncertainty of this isochron, after reprocessing the data, we obtained an isochron age for 4 chalcopyrite samples of  $430 \pm 15$  Ma (MSWD = 0.53). Two sample sets have a similar age, but the latter has a smaller uncertainty. This result may be due to different samples containing different initial Os values. Thus, the Re–Os isochron age of 432 Ma is interpreted to represent the age of vein mineralization of the Huangtan Au–Cu–Zn deposit. The veins occasionally crosscut the layered orebody, indicating that the formation time of the vein orebody is later than that of the layered orebody. The chalcopyrite isochron age of 432 Ma is consistent with that of the pyrite isochron Re–Os age (438 Ma) and zircon U–Pb age (438 Ma; Sun et al. 2020) of the tuff in the Huangtan deposit. Therefore, the age of the mineralization of the Huangtan deposit should be approximately Early Silurian. Mantle rock has  $^{187}\text{Os}/^{188}\text{Os}$  ratios similar to those of chondrites (0.127–0.129; Walker and Morgan 1989; Meisel et al. 1996), while the crust has abnormally high  $^{187}\text{Os}/^{188}\text{Os}$  ratios (3.63; Palmer and Turekian 1986). Therefore, the initial  $^{187}\text{Os}/^{188}\text{Os}$  ratios are a good tracer for distinguishing mantle-derived and crust-derived rocks. This analysis shows that the initial  $^{187}\text{Os}/^{188}\text{Os}$  ratio of the four chalcopyrite Re–Os isotope systems is  $0.55 \pm 0.94$  in the Huangtan deposit, which is significantly higher than the mantle  $^{187}\text{Os}/^{188}\text{Os}$  ratio of 0.129 and lower than the crust  $^{187}\text{Os}/^{188}\text{Os}$  ratio of 3.63. The ore-forming fluids originated from the mantle, and crust-derived materials were added. Plate subduction may be a way of adding crustal materials (Sun et al. 2020).

## Nature of the ore-forming fluids and sources

### Nature of the ore-forming fluids

Fluid inclusions in the Huangtan Au–Cu–Zn deposit are dominated by L-type, P-type, and rare V-type fluid inclusions, suggesting that the ore-forming fluids belonged to a salt–water system. The characteristics of the fluid inclusions are similar to those of most VMS deposits (Ulrich et al. 2002; Zaw et al. 2003). The majority of the homogenization temperatures of fluid inclusions in quartz from altered wall rock and of vein mineralization are mainly 120–340 °C, with a peak at approximately 230 °C (Fig. 11A), and 120–300 °C, with a peak at

approximately 130 °C (Fig. 11C), respectively. The majority of salinities for fluid inclusions in altered wall rock and vein mineralization mainly range from 2 to 7 wt% NaCl equiv. (Fig. 11B) and 1 to 9 wt% NaCl equiv., respectively (Fig. 11D). The salinities of fluids in quartz from vein mineralization are similar to those of fluids from altered wall rock.

The temperature and salinity ranges of the fluid inclusions in the stockwork unit of the Huangtan deposit are similar to those of fluid inclusions in the stockwork unit of other VMS deposits, such as the Honghai–Huangtupo (108–400 °C and 2.4–13.7 wt% NaCl equiv.; Yang et al. 2018a; Mao et al. 2019; Cheng et al. 2020a), Ashele (117–514 °C and 0.7–12.3 wt% NaCl equiv.; Yang et al. 2018b), Sarsuk (130–390 °C and 3.0–10.0 wt% NaCl equiv.; Yang 2017), Xiaotieshan (174–452 °C and 0.7–10.7 wt% NaCl equiv.; Liang et al. 2016), Hellyer (165–322 °C and 3.0–15.0 wt% NaCl equiv.; Zaw et al. 1996) and Mt Morgan (172–276 °C and 0.2–15.3 wt% NaCl equiv.; Eadington et al. 1974; Ulrich et al. 2002) VMS deposits.

The majority of homogenization temperatures of fluid inclusions in barite from barite-bearing pyrite ore range between 140 and 260 °C, and the salinities range from 3 to 9 wt% NaCl equiv (Fig. 11E, F). Data for the measured inclusions are few and the results are for reference only. In the Huangtan deposit, the temperatures of fluid inclusions in barite-bearing pyrite ore are higher than those in vein mineralization. A comparison of the temperatures and salinities of fluid inclusions from the exhalative–sedimentary units of other VMS deposits, such as the Ashele (122–537 °C and 1.6–10.5 wt% NaCl equiv.; Yang et al. 2018b), Honghai–Huangtupo (99–377 °C and 9.3–18.2 wt% NaCl equiv.; Mao et al. 2014; Yang et al. 2018a; Mao et al. 2019; Cheng et al. 2020a), Xiaotieshan (149–388 °C and 2.2–14.6 wt% NaCl equiv.; Liang et al. 2016), and Mt. Morgan (200–246 °C and 0.7–8.3 wt% NaCl equiv.; Eadington et al. 1974; Ulrich et al. 2002) VMS deposits, show that they have similar temperature and salinity ranges. Microthermometry data are plotted to generate a diagram of homogenization temperature vs. salinity, which illustrates the similarities between this deposit and other Au-rich VMS-type deposits (Fig. 12). The salinities are mostly in the range of 2–6 wt%, and the homogenization temperatures of fluid inclusions range from  $\leq 100$  to  $\sim 360$  °C in VMS-type deposits (Bodnar et al. 2014). The results imply that their temperature range values are wide and do not concentrate in a narrow range, while the salinity values are usually concentrated in a narrow range. The fluids have a wide range of temperatures, which may be caused by the intermittent and/or continuous ascent of magmatic hydrothermal fluids and their mixing with seawater.



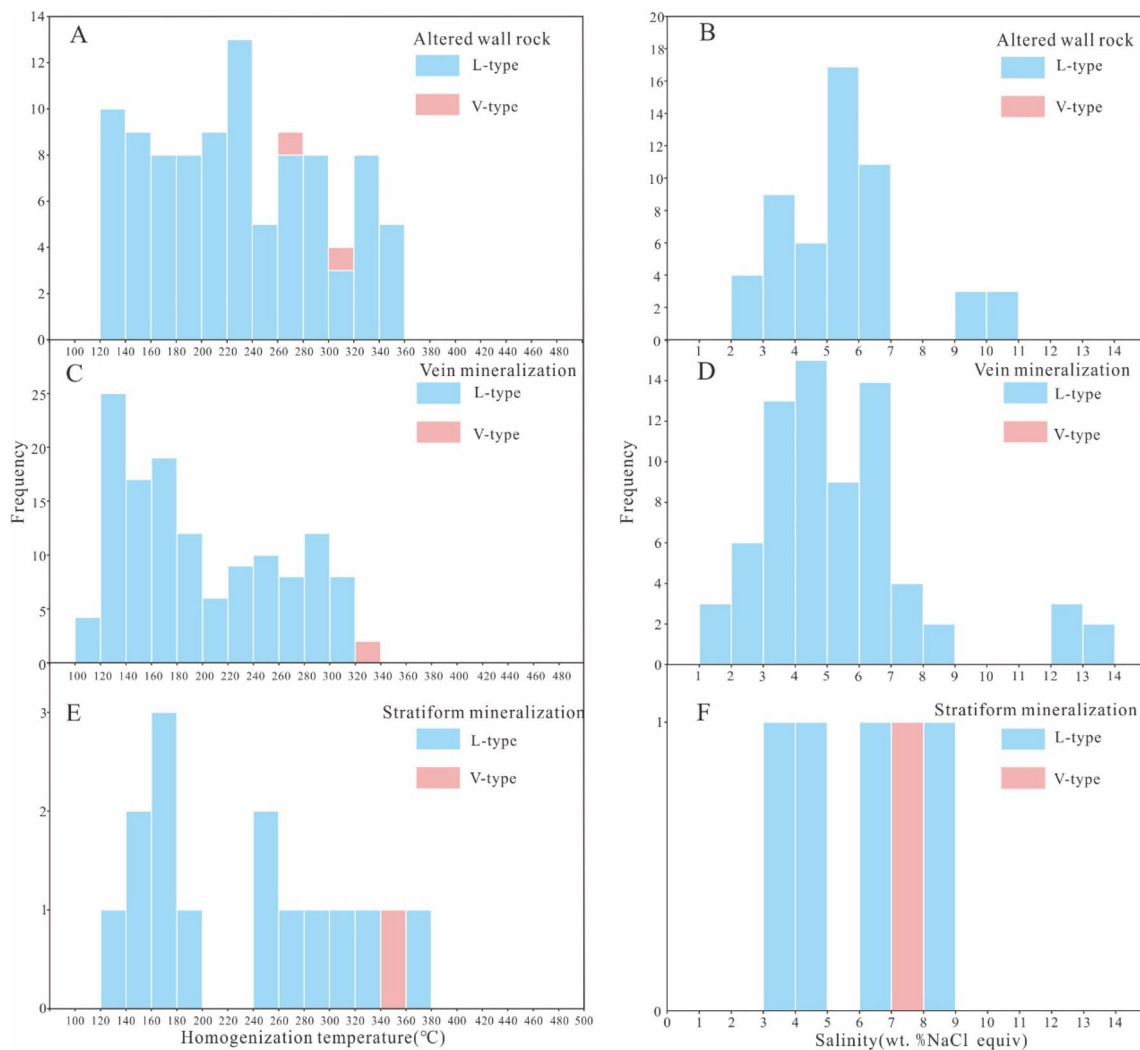


**Fig. 11** Histograms of homogenization temperatures and salinities of fluid inclusions

### Sources of the ore-forming fluids

The isotopic compositions of H and O are commonly employed to trace the source of ore-forming fluids. The  $\delta D_{V-SMOW}$  values of quartz-hosted and barite-hosted fluid inclusions from the Huangtan Au–Cu–Zn deposit range from  $-69$  to  $-42\text{‰}$  and mainly overlap with those of primary magmatic fluids ( $\delta D_{V-SMOW} = -50\text{‰}$  to  $-85\text{‰}$ ; Taylor 1974). The range of  $\delta^{18}O_{fluid}$  values is relatively large, with the majority of the  $\delta^{18}O_{fluid}$  values ranging from  $-7.24$  to  $6.81\text{‰}$ . These values fall between those of primary magmatic waters ( $\delta^{18}O_{fluid} = 5.5\text{‰}$  to  $10.0\text{‰}$ ; Taylor 1974) and meteoric water, and some values fall in the range of magmatic waters, suggesting that the addition of meteoric water to ore-forming fluids changes the  $\delta^{18}O_{fluid}$  value. Compared to the Honghai–Huangtupo ( $\delta D_{V-SMOW} = -109$  to  $-48\text{‰}$  and  $\delta O_{H_2O} = -3.2$  to  $4.0\text{‰}$ ; Yang et al. 2018a; Mao et al. 2019), Sarsuk ( $\delta D_{V-SMOW} = -140$  to  $-92\text{‰}$  and  $\delta O_{H_2O} = -4.5$

to  $0.9\text{‰}$ ; Yang 2017), and Xiaotieshan ( $\delta D_{V-SMOW} = -153$  to  $-88\text{‰}$  and  $\delta^{18}O_{fluid} = -1.1$  to  $4.6\text{‰}$ ; Liang et al. 2016) deposits, the Huangtan deposit has a higher  $\delta D_{V-SMOW}$  value and a wider range of  $\delta^{18}O_{fluid}$  values. In the  $\delta D_{V-SMOW}$  vs.  $\delta^{18}O_{fluid}$  diagram (Fig. 13), the data illustrate the similarities between  $\delta D_{V-SMOW}$  and  $\delta^{18}O_{fluid}$  values of the Huangtan and other VMS deposits in adjacent regions (e.g., the Ashele, Honghai–Huangtupo, Sarsuk, and Xiaotieshan deposits) and elsewhere in the world (e.g., Rio Tinto and Horne deposits). All sample points plot within the region between meteoric water and primary magma water. The Huangtan Au–Cu–Zn deposit formed at or near the seafloor, and the effects of meteoric water can be neglected. The data may represent deeply circulating seawater. The H–O isotope data imply that the ore-forming fluids were a mixture of magmatic fluids and deeply circulating seawater.

The marked differences in the isotopic composition of the noble gases can be employed as tracers for crust and mantle

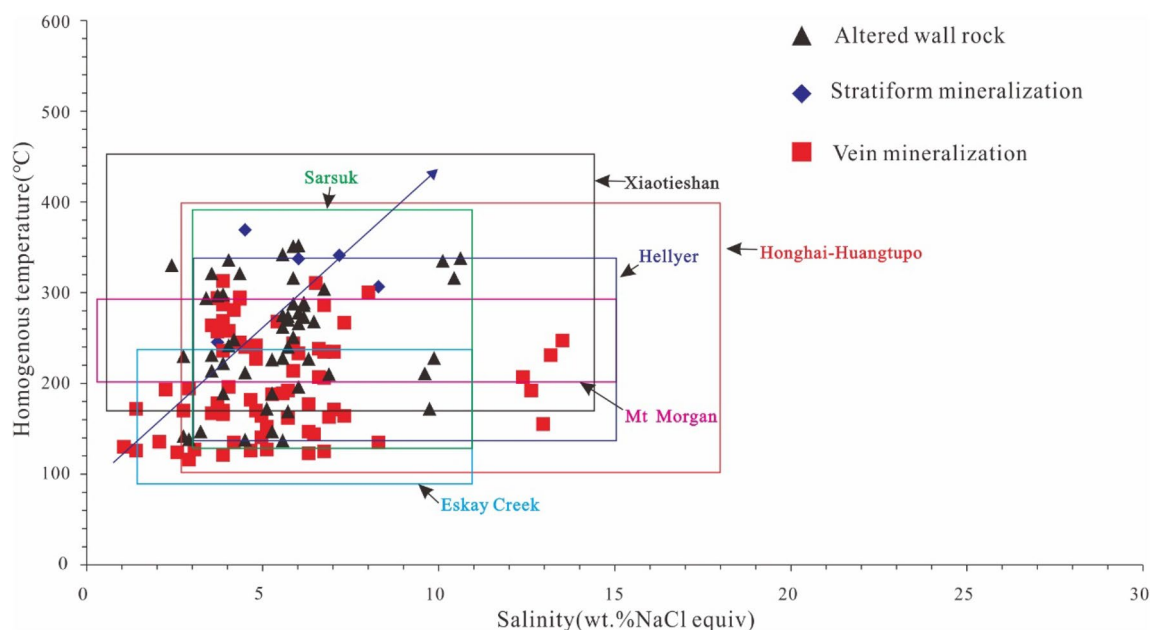


**Fig. 12** Salinity vs. homogenization temperature illustrating the distribution pattern of the data points from the Huangtan Au–Cu–Zn deposit, data of Hellyer after Zaw et al. (1996), data of Eskay Creek after Sherlock et al. (1999), data of Mt Morgan are after Ulrich et al.

(2002) and Eadington et al. (1974), data of Xiaotieshan after Liang et al. (2016), data of Sarsuk after Yang. (2017), data of Honghai–Huangtupo after Mao et al. (2014), Yang et al. (2018a) and Mao et al. (2019)

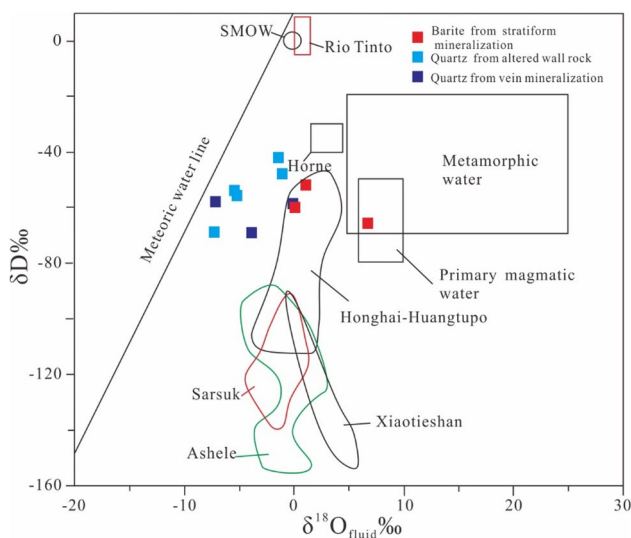


**Fig. 13**  $\delta D_{V-SMOW}-\delta^{18}O_{fluid}$  diagram of the VMS deposit (modified after Sheppard 1986), data of Rio Tinto, Horne after Huston (1999) and the references therein, data of Xiaotieshan after Liang et al. (2016), data of Sarsuk after Yang (2017), data of Ashele after Yang et al. (2018b), data of Honghai–Huangtupo after Yang et al. (2018a) and Mao et al. (2019)

contributions to the ore-forming fluids (Sano and Wakita 1985). In general, inclusion-trapped He and Ar isotopes have three potential sources: air-saturated water (ASW), with  $^3\text{He}/^4\text{He}$  ratios of  $1.4 \times 10^{-6}$  (1 Ra) and a  $^{40}\text{Ar}/^{36}\text{Ar}$

ratio of 295.5; mantle-derived fluids, with  $^3\text{He}/^4\text{He}$  ratios of 6–9 Ra and  $^{40}\text{Ar}/^{36}\text{Ar} > 40,000$ ; and crust-derived fluids, with  $^3\text{He}/^4\text{He}$  ratios of 0.01–0.05 Ra and  $^{40}\text{Ar}/^{36}\text{Ar} > 45,000$ . Mantle-derived Ar and crust-derived Ar are dominated by radiogenic  $^{40}\text{Ar}$  ( $^{40}\text{Ar}^*$ ), showing that  $^{40}\text{Ar}/^{36}\text{Ar}$  ratios are extremely high in mantle-derived and crust-derived fluids (Turner et al. 1993; Stuart et al. 1995; Hu 1997; Burnard et al. 1999).

Pyrite in the Huangtan Au–Cu–Zn deposit was collected from underground workings; therefore, the effect of cosmogenic He can be excluded (Simmons et al. 1987; Stuart et al. 1995). In the analysis, the atmospheric He contribution can be estimated by  $F^4\text{He}$  (Kendrick et al. 2001), which is the ratio of  $^4\text{He}/^{36}\text{Ar}$  in the sample relative to  $^4\text{He}/^{36}\text{Ar}$  in the atmosphere (0.165). If the sample contains 100% atmospheric He, then  $F^4\text{He} = 1$ . The  $F^4\text{He}$  values (2405–8570) of the Huangtan pyrite samples are far greater than 1, indicating that atmospheric helium had no influence.

The  $^3\text{He}/^4\text{He}$  ratios of fluid inclusions in pyrite from vein mineralization are 0.929 and 1.374 (R/Ra), and the ratio of fluid inclusions in pyrite from massive chalcopyrite–pyrite ore is 1.226 (R/Ra), which are both 20–130 times higher than those of the crust (0.01–0.05 R/Ra; Stuart et al. 1995) but 6–9 times lower than those of the mantle (6–9 R/Ra). The low He solubility in ASW hardly influences the He isotope compositions of most mantle or crustal fluids (Marty et al. 1989; Stuart et al. 1994). In the  $^3\text{He}$  vs.  $^4\text{He}$  diagram, the He isotope composition data points are distributed

between the mantle and crustal He domains (Fig. 14A). The percentage of mantle-derived He in hydrothermal fluid can be calculated according to the crust–mantle dual model (Kendrick et al. 2001). The calculation results for the percentage of mantle-derived He from the Huangtan Au–Cu–Zn deposit vary from 14.02 to 20.9% (mean 17.84%). These values are higher than those of the Honghai–Huangtupo deposit (1.71–10.97%; Chai et al. 2017). Consequently, the He isotope results show that the ore fluids in the Huangtan Au–Cu–Zn deposit were dominated by crust-derived fluids and some mantle-derived fluids.

The  $^{40}\text{Ar}/^{36}\text{Ar}$  ratios of ore-forming fluids in the Huangtan Au–Cu–Zn deposit range from 388 to 502, which are higher than those of ASW Ar ( $^{40}\text{Ar}/^{36}\text{Ar} = 295.5$ ). The ratio values indicate the existence of radiogenic  $^{40}\text{Ar}$  originating from the mantle or crust. The proportion of radiogenic  $^{40}\text{Ar}$  can be estimated (Kendrick et al. 2001). The calculated  $^{40}\text{Ar}^*$  concentration ranges from 23.8 to 41.1%. The  $^{40}\text{Ar}/^4\text{He}$  ratios of ore-forming fluids are 0.836–1.157, namely, the  $^{40}\text{Ar}^*/^4\text{He}$  ratios of vein mineralization range from 0.146 to 0.412, and the  $^{40}\text{Ar}^*/^4\text{He}$  ratio of massive ore is 0.146. These values are near the crustal production  $^{40}\text{Ar}^*/^4\text{He}$  ratio of 0.2 and lower than the mantle  $^{40}\text{Ar}^*/^4\text{He}$  ratio of 0.69 (Stuart et al. 1995), indicating that the ore fluids were mainly derived from the crust and partially derived from the mantle.

On the R/Ra vs.  $^{40}\text{Ar}/^{36}\text{Ar}$  diagrams (Fig. 14B), the data points plot near the ASW Ar data, suggesting that ASW Ar entered the ore-forming fluids. The  $^{40}\text{Ar}/^{36}\text{Ar}$  ratios are similar to those of the Huangtupo, Ashele, Dao Bao Hill, and Wetar VMS deposits and the Trans-Atlantic Geotraverse (TAG) of the Mid-Atlantic Ridge. The fluids of these deposits are considered a mixture of mantle fluid and seawater. The He–Ar isotope characteristics of the Huangtan Au–Cu–Zn deposit suggest that the ore-forming fluids were a mixture of mantle fluids with seawater containing crustal He and atmospheric Ar.

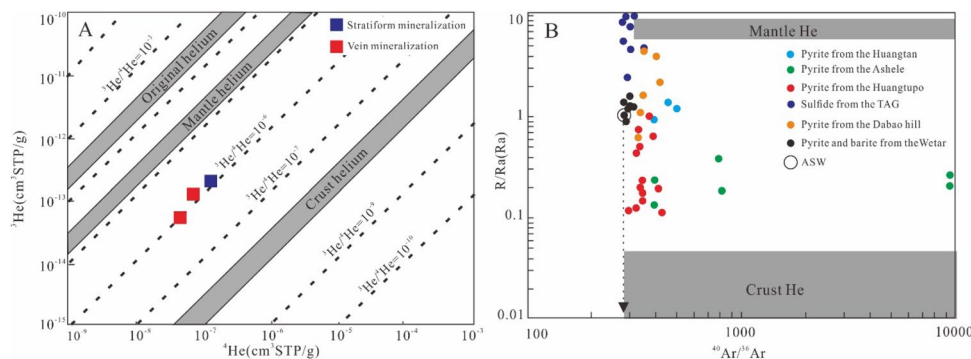


**Fig. 14** Helium isotope composition of fluid inclusions in pyrite from the Huangtan Au–Cu–Zn deposit (A) (modified after Mamyryn and Tolstikhin 1984) and Plot of  $^3\text{He}/^4\text{He}$ – $^{40}\text{Ar}/^{36}\text{Ar}$  ratios of the fluids in pyrite of the VMS-type deposit (B), data of TAG after Zeng

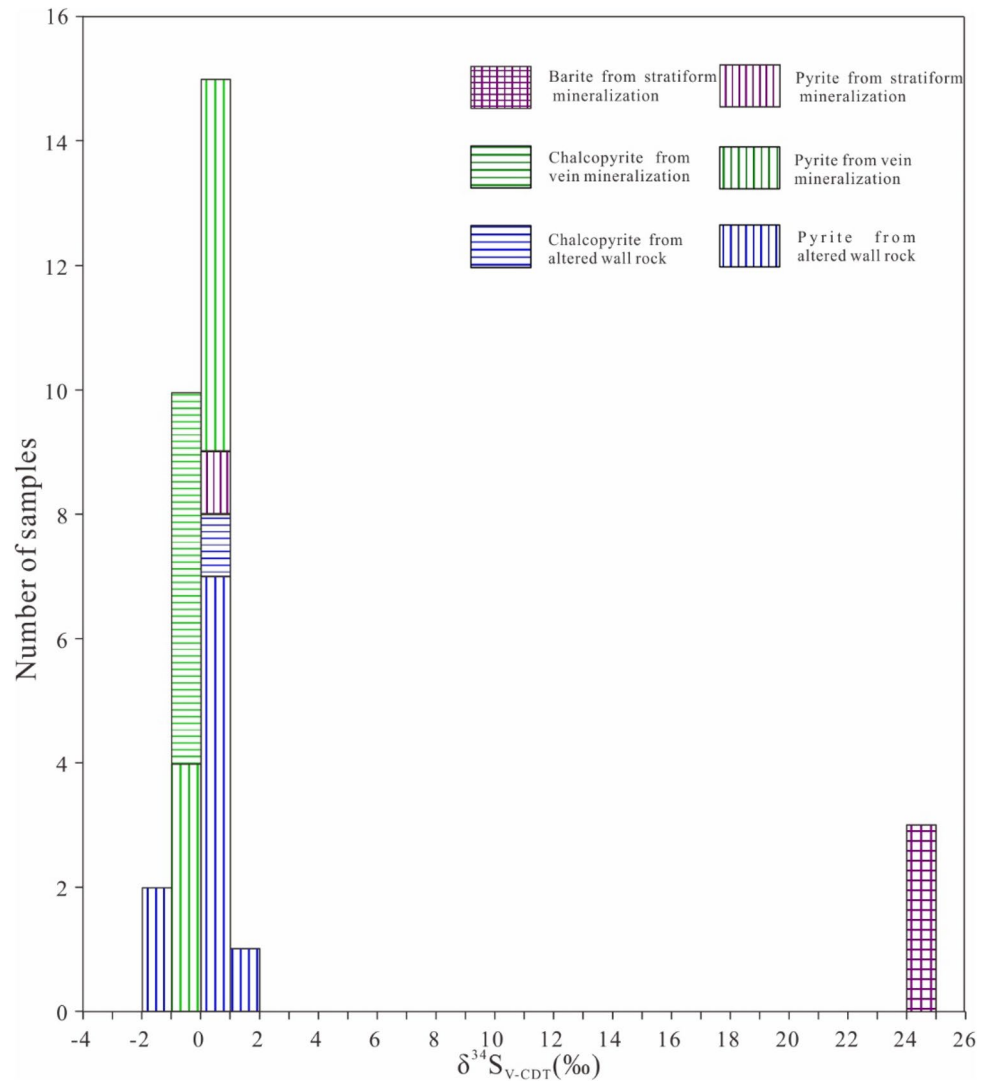
## Sources of sulfur

Studies have shown that three main sources of sulfur are common in VMS deposits (Hoefs 2009; Shanks 2001; Brueckner et al. 2016): (1) seawater sulfate reduced by thermochemical processes ( $\delta^{34}\text{S} \approx 4$  to  $33\text{‰}$ ), (2) direct sulfur contributions from magmatic fluids and/or leaching from igneous footwall rocks ( $\delta^{34}\text{S} \approx -5$  to  $5\text{‰}$ , averaging  $0\text{‰}$ ), and (3) bacterial reduction of seawater sulfate ( $\delta^{34}\text{S} \approx -50$  to  $20\text{‰}$ ). The mean  $\delta^{34}\text{S}_{\text{V-CDT}}$  values of pyrite and chalcopyrite from the altered wall rock are  $0.3\text{‰}$  and  $0.2\text{‰}$ , respectively; the values of pyrite and chalcopyrite from vein mineralization are  $0.2\text{‰}$  and  $-0.7\text{‰}$ , respectively; and the value of pyrite of massive ore is  $0.4\text{‰}$  in the Huangtan deposit. The values of the altered wall rock, vein mineralization and massive ore are similar and have a narrow range, implying that they have a homogeneous sulfur source (Fig. 15; Ohmoto and Rye 1979). However, the  $\delta^{34}\text{S}_{\text{V-CDT}}$  values themselves do not require a detectable input of bacteriogenic sulfide or reduction of seawater sulfate that exhibits a wide range of values, because they are narrow in range ( $-2.0$  to  $1.5\text{‰}$ ) and consistent with the mantle sulfur value ( $0 \pm 3\text{‰}$ ; Hoefs 2009). This result is similar to those for VMS Cu–Zn deposits in the Kalatag area and VMS deposits in other areas (Fig. 16A).

Under thermodynamic equilibrium conditions, the relative order of  $^{34}\text{S}$  enrichment is sulfate species  $\gg$  sulfide minerals. Three analyzed barite samples yield  $\delta^{34}\text{S}_{\text{V-CDT}}$  values of  $24.1$ – $24.8\text{‰}$ . The  $\delta^{34}\text{S}_{\text{V-CDT}}$  values of barite differ from those of sulfides by  $\sim 24\text{‰}$ . This difference is close to the isotopic fractionation between aqueous sulfur and sulfide at temperatures of  $250$ – $400$  °C ( $19$ – $25\text{‰}$ ; Ohmoto et al. 1983; Solomon et al. 1988; Huston 1999). We believe that the formation of barite is mainly related to the disproportionation of  $\text{SO}_2$  inherited from the magmatic source:  $3\text{SO}_2 + 3\text{H}_2\text{O} = \text{S}^0 + 2\text{H}^+ + 2\text{HSO}_4^-$ ,  $\text{HSO}_4^- = \text{H}^+ + \text{SO}_4^{2-}$ ,  $\text{BaSO}_4 = \text{Ba}^{2+} + \text{SO}_4^{2-}$ . The  $\delta^{34}\text{S}_{\text{V-CDT}}$  values of the barite

et al. (2000), data of the Wetar after Herrington et al. (2011), data of Dabao hill after Song et al. (2007), data of Huangtupo after Chai et al. (2017), data of Ashele after Yang et al. (2018b)

**Fig. 15** Histogram of sulfur isotopic compositions of the Huangtan Au–Cu–Zn deposit



in the Huangtan deposit are similar to those of barite in the Honghai–Huangtupo deposit (Fig. 16B, Yang et al. 2018a). It is reasonable to conclude that they have similar sulfur sources. The sulfur isotopes of sulfide from the Huangtan deposit could indicate magmatic sulfur as a major source of sulfur, which is consistent with those of a typical VMS-type deposit (Franklin et al. 2005).

### Au–Cu–Zn metallogensis

According to the grade and content of Au and gold-to-base metal ratios, the deposit can be divided into three categories: anomalous ( $\geq 31$  metric tons of Au), auriferous (Au grade  $> 3.46$  g/t and/or gold-to-base metal ratio  $> 1$ ) and Au-rich (Au grade  $> 3.46$  g/t and/or gold-to-base metal ratio  $> 1$  and  $> 31$  metric tons of Au) VMS deposits (Mercier-Langevin et al. 2011). The AuCu1 orebody and CuZn2 orebody are the principal orebodies in the Huangtan deposit. The Au average grade of the AuCu1 orebody is 4.07 g/t, and

the gold-to-base metal ratio is 5.21. The CuZn2 orebody includes ores of Cu and Zn, accompanied by Au. The average Au grade of the CuZn2 orebody is 0.7 g/t and the gold-to-base metal ratio is 0.3; therefore, the AuCu1 orebody is an auriferous orebody. Au in the Honghai–Huangtupo deposit is concentrated in massive ore bodies, along with the associated elements (Mao et al. 2016). The average Au grade of the Honghai–Huangtupo deposit is 0.6 g/t, and the gold-to-base metal ratio is  $< 1$  (Deng et al. 2018b). The Honghai–Huangtupo deposit is not considered as an auriferous VMS deposit. In the Huangtan deposit, gold occurs mainly in the vein orebody of the stockwork unit, and a small amount of gold occurs in the massive orebody of the exhalative–sedimentary units. The vein orebody is unconformably in contact with the layered orebody, and ore veins occasionally crosscut the layered orebody. We conclude that the Huangtan deposit is an auriferous syngenetic VMS deposit.

VMS deposits can form in a variety of tectonic settings, including nascent arc, rifted arc, back-arc, seafloor

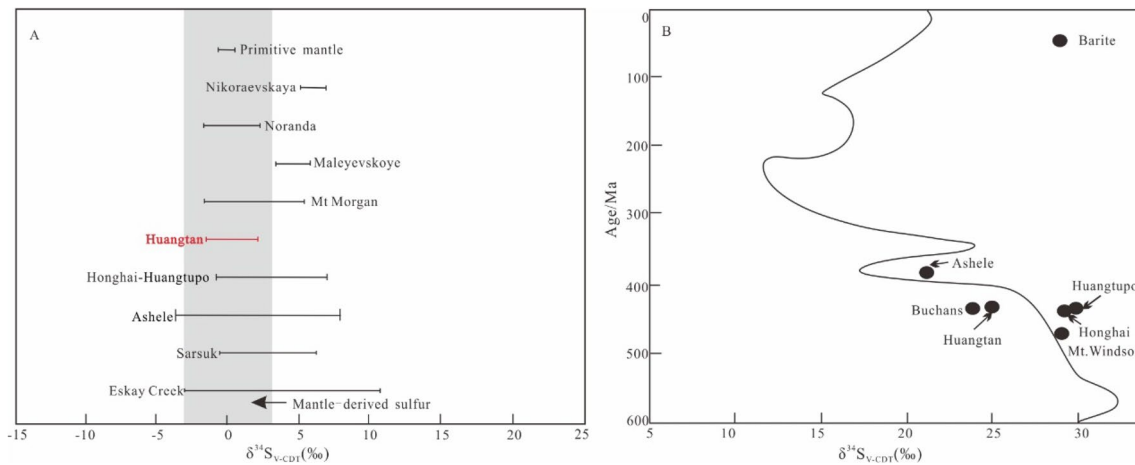


**Fig. 16** Comparison with  $\delta^{34}\text{S}_{\text{V-CDT}}$  values of sulfide minerals in typical VMS deposits (A), data of Eskay Creek after Sherlock et al. (1999), data of Mt Morgan after Ulrich et al. (2002), data of Noranda after Chen et al. (2014), data of Honghai–Huangtupo after Mao et al. (2015a, b) and Yang et al. (2018a), data of Nikoraevskaya, Maleyevskoye, data of Ashele after Yang et al. (2018b) and  $\delta^{34}\text{S}_{\text{V-CDT}}$  values of

marine sulphate in different geological times (B) (modified after Seal et al 2000), data of Buchans, Mt. Windsor after Huston (1999) and the references therein, data of Honghai after Mao et al. (2015b), data of Huangtupo after Yang et al. (2018a), data of Ashele after Yang et al. (2018b)

spreading centers and rifted continental margin environments (Franklin et al. 2005). The subduction of the oceanic plate during the Late Ordovician–Silurian formed the Dananhu island arc associated with magmatic events (Xiao et al. 2004; Chai et al. 2019; Mao et al. 2019). During this period, VMS deposits formed in the Kalatag area, such as the Honghai–Huangtupo VMS Cu–Zn deposit (isochron age of 432–439 Ma; Deng et al. 2016; Yang et al. 2018a; Mao et al. 2019; Cheng et al. 2020a) and the Hongshi volcano-hydrothermal vein-type Cu deposit (Re–Os isochron ages of 432 Ma; Deng et al. 2016). The ages of these deposits are similar to the age of the Huangtan deposit. The Huangtan deposit adjoins the Honghai–Huangtupo and Hongshi deposits and all three deposits have similar geological backgrounds of mineralization, and metal associations (Yang et al. 2018a; Chai et al. 2019; Mao et al. 2019; He 2019; Cheng et al. 2020a; Sun et al. 2020). Therefore, these deposits may be affected by volcanic activity in the same period, and thus formed in the same metallogenic system. The VMS mineralization is controlled by volcanic slopes, depressions and recharge channels, and volcanic hydrothermal Cu deposits are controlled by volcanic faults and fissures (Deng et al. 2016; Chai et al. 2019; Cheng et al. 2020b). Faults may also allow seawater to penetrate volcanic rock and mix with magmatically generated metalliferous fluid. The metallogenic materials are mainly derived from deep magmas and transported as sulfide complexes in the ore-forming fluids at low temperatures (Barnes 1979). Gold transport as  $\text{Au}(\text{HS})^-$  occurs at relatively low temperatures (< 300 °C) (Huston and Large 1989). Under the conditions

of  $\text{Au}(\text{HS})^-$  transport, the most effective method of depositing gold is to decrease the activity of reduced sulfur. The activity of reduced sulfur may be decreased by precipitation of metal sulfides, dilution or boiling (Seward 1984). When magmatic fluids mix with seawater, they cause metal precipitation and dilution in ore-forming fluids (Huston and Large 1989). Barite in the massive ore formed as reduced hydrothermal fluid carrying Ba mixed with seawater containing sulfate. Tellurium is likely to be of magmatic origin and Au may also migrate as  $\text{Au}(\text{HTe}_2)^-$  complexes (Patten et al. 2015; Seward 1973). A comparison of the fluid inclusion characteristics of the Huangtan deposit and the Honghai–Huangtupo deposit shows that the Huangtan deposit lacks daughter-mineral-bearing multiphase inclusions (S-type), and inclusions with  $\text{H}_2\text{O}$ – $\text{CO}_2$  liquid phase inclusions (C-type) (Mao et al. 2014; Yang et al. 2018a; Mao et al. 2019; Cheng et al. 2020a). Fluid boiling results in a marked loss of volatiles, such as  $\text{N}_2$  and  $\text{CO}_2$  (Hedenquist et al. 1998; Simmons et al. 2005). The V- and L-types coexist and have similar homogenization temperatures, indicating local fluid immiscibility or boiling in the stockwork unit of the Honghai–Huangtupo deposit; however, immiscibility or boiling does not occur in the exhalative–sedimentary units in the Honghai–Huangtupo deposit (Cheng et al. 2020a). According to recent fluid inclusions research on the Huangtan deposit, few V-type fluid inclusions exist in the Huangtan deposit. A few V- and L-type fluid inclusions coexist; however, their homogenization temperatures vary greatly, indicating that local fluid is not immiscible or boils in the Huangtan deposit. The fluid inclusions of the massive orebodies

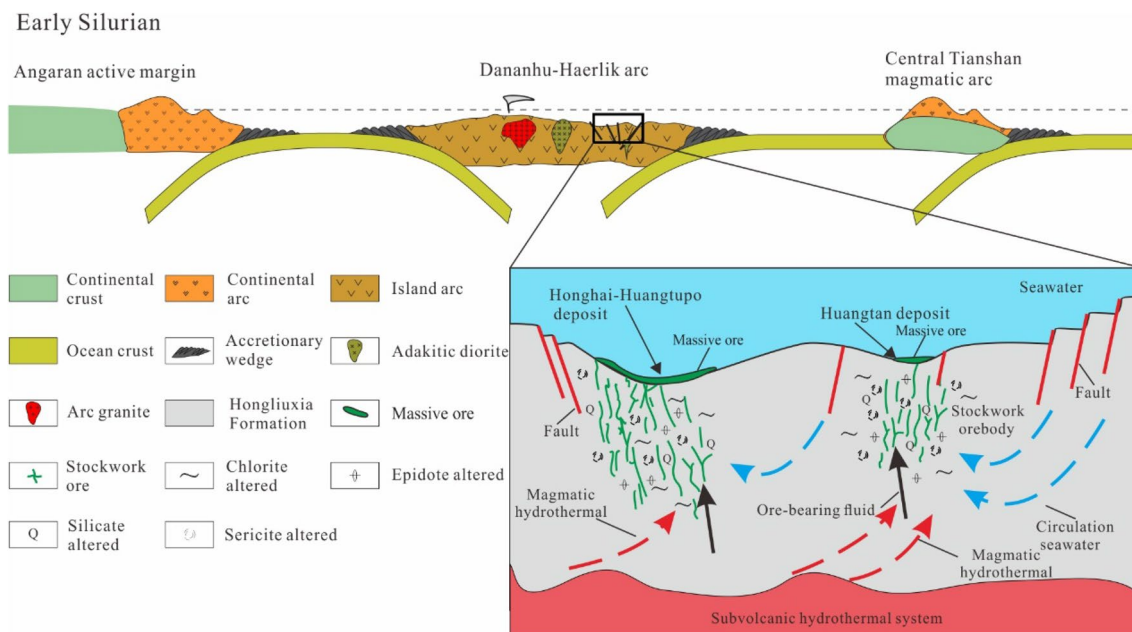


**Fig. 17** Schematic diagram illustrating the tectonic setting and possible genetic model of the Huangtan deposit. The tectonic setting is modified after Mao et al. (2019)

and stockwork orebodies in the Honghai–Huangtupo VMS Cu–Zn deposit yield homogenization temperatures with peak values of 265 °C, and 350 °C, respectively (Cheng et al. 2020a). The peak temperature of the fluid inclusions is 130 °C in the vein mineralization of the Huangtan deposit, which is less than that of the Honghai–Huangtupo deposit. Except for the Huangtan deposit containing native gold and auriferous tellurides, the Huangtan deposit and the Honghai–Huangtupo deposit have similar mineral associations. In addition, the formation of tellurides is sensitive to the temperature of the mineralization system, and as the temperature of the ore-forming system continues to decrease, the tellurium fugacity required for the formation of telluride also continues to decrease (Afifi et al. 1988; Brueckner et al. 2016). We conclude that gold precipitation may have been more closely related to decreasing temperature caused by the mixing of magmatic fluid and seawater.

The ore-forming mechanism is schematically shown in Fig. 17. The ore-forming fluids migrated upwards along a volcanic conduit driven by the magmatic hydrothermal system during a volcanic hiatus. Changes in the physico-chemical conditions (decreasing temperature and pressure) of the ore-forming fluids when vented within the seafloor resulted in the precipitation of sulfides and gold, forming layered ore bodies within depressions on the seafloor and veinlet, and stockwork mineralization in the stockwork unit. Volcanic breccia buried the layered orebodies during the later volcanism.

## Conclusions

- (1) The Huangtan Au–Cu–Zn deposit is an auriferous VMS deposit that is hosted in the volcanic breccia and tuff of the Hongliuxia Formation. The orebodies are composed of layered, layered-like orebodies and stockwork orebodies.
- (2) The  $^{187}\text{Re}/^{188}\text{Os}$  vs.  $^{187}\text{Os}/^{188}\text{Os}$  isochron age of 432 Ma obtained from chalcopyrite represents the ore-forming age of the Huangtan Au–Cu–Zn deposit. The Huangtan, and Honghai–Huangtupo deposits in the Kalatag area are products of the same metallogenic system.
- (3) The ore-forming fluids of the Huangtan deposit belonged to a simple  $\text{H}_2\text{O}$ – $\text{NaCl}$  system. The He and Ar isotope compositions and H–O isotopes imply that the ore-forming fluids were a mixture of magmatic fluids and deeply circulating seawater. The sulfur isotopes suggest that magmatic sulfur was the main source of sulfur in the ore-forming fluids.
- (4) Decreases in the temperature and pressure of ore-forming fluids played important roles in the ore-forming processes of the Huangtan Au–Cu–Zn deposit.

**Acknowledgements** This research was supported by the National Key R&D Program of China (Grant no. 2017YFC0601201), the National Natural Science Foundation of China Program (Grant no. 42072100) and the Dynamic evaluation of mineral resources potential in China (Grant no. DD20190193). We are grateful to the technicians and leaders of the Xituo Mining Corporation, Xinjiang Uygur Autonomous

Region, for their help with field work. We thank Chao Li, Huiyan Zhu, Defang Wan, Zengjie Zhang, Feng Liu, Jianfei Gao, Xihui Cheng and Ning Li for laboratory and field work assistance.

## Declarations

**Conflict of interest** The authors declare that they have no known competing financial interests or personal relationships that could have appeared to influence the work reported in this paper.

## References

- Afifi AM, Kelly WC, Essene EJ (1988) Phase relations among tellurides, sulfides, and oxides: part II. Applications to telluride-bearing ore deposits. *Econ Geol* 83:395–404
- Barnes HL (1979) Solubilities of ore minerals. *Geochem Hydrothermal Ore Deposits* 2:404–460
- BGMRXUAR (Bureau of Geology and Mineral Resources of Xinjiang Uygur Autonomous Region) (1993) *Regional Geology of the Xinjiang Uygur Autonomous Region*, Beijing: Geological Publishing House. pp: 1–841 (in Chinese)
- Bodnar RJ (1993) Revised equation and table for determining the freezing point depression of H<sub>2</sub>O–NaCl solutions. *Geochim Cosmochim Acta* 57:683–684
- Bodnar RJ, Lecumberri-Sanchez P, Moncada D, Steele-MacInnis M (2014) Fluid inclusions in hydrothermal ore deposits. In: Holland HD, Turekian KK (eds) *Treatise on geochemistry*, vol 13, 2nd edn. Elsevier, Amsterdam, pp 119–142
- Bruceckner S, Piercey S, Pilote JL, Layne G, Sylvester P (2016) Mineralogy and mineral chemistry of the metamorphosed and precious metalbearing Ming deposit, Canada. *Ore Geol Rev* 72:914–939
- Burnard PG, Hu RZ, Turner G, Bi XW (1999) Mantle, crustal and atmospheric noble gases in Ailaoshan gold deposit, Yunnan province, China. *Geochim Cosmochim Acta* 63:1595–1604
- Chai FM, Xu QF, Wang W, Wang HP (2017) Helium and argon isotope characteristics of ore-forming fluids for the Huangtupo copper-zinc deposit, eastern Tianshan. *Chin J Geol* 52(4):1263–1281 (in Chinese with English abstract)
- Chai FM, Zhang ZC, Li WH, Santosh M, Wang HP, Wang W, Xu QF (2019) The early Paleozoic Huangtupo VMS Cu–Zn deposit in Kalatag, Eastern Tianshan: implications from geochemistry and zircon U–Pb geochronology of volcanic host rocks. *Lithos* 342–343:97–113
- Chen YJ, Pirajno F, Wu G, Qi JP, Xiong XL, Zhang L (2012) Epithermal deposits in north Xinjiang, NW China. *Int J Earth Sci* 101:889–917
- Chen H, Ni P, Wang RC, Wang GG, Zhao KD, Ding JY, Zhao C, Cai YT, Xu YF (2014) A combined fluid inclusion and S–Pb isotope study of the Neoproterozoic Pingshui volcanogenic massive sulfide Cu–Zn deposit, Southeast China. *Ore Geol Rev* 66:388–402
- Chen L, Wang JB, Bagas L, Wu XB, Zou HY, Zhang HQ, Sun Y, Lv XQ, Deng XH (2017) Significance of adakites in petrogenesis of early Silurian magmatism at the Yudai copper deposit in the Kalatag district, NW China. *Ore Geol Rev* 91:780–794
- Chen ZY, Xiao WJ, Windley BF, Schulmann K, Mao QG, Zhang ZY, Zhang JE, Deng C, Song SH (2019) Composition, provenance and tectonic setting of the Southern Kangurtag accretionary complex in the Eastern Tianshan, NW China: Implications for the late Paleozoic evolution of the North Tianshan Ocean. *Tectonics* 38:2779–2802
- Chen L, Deng XH, Bagas L, Wu XB, Zou HY, Zhang HQ, Sun Y, Lv XQ, Wang JB (2020) Petrogenesis of Middle Devonian diorite at the Xierqu Fe–Cu deposit in the Kalatag district, eastern Tianshan, NW China. *Geol J* 55:1620–1635
- Cheng XH, Yang FQ, Zhang R, Yang CD (2019) Hydrothermal evolution and ore genesis of the Hongshi copper deposit in the East Tianshan Orogenic Belt, Xinjiang, NW China: Constraints from ore geology, fluid inclusion geochemistry and H–O–S–He–Ar isotopes. *Ore Geol Rev* 109:79–100
- Cheng XH, Yang FQ, Zhang R, Xu QF, Li N (2020a) Metallogenesis and fluid evolution of the Huangtupo Cu–Zn deposit, East Tianshan, Xinjiang, NW China: constraints from ore geology, fluid inclusion geochemistry, H–O–S isotopes, and U–Pb zircon, Re–Os chalcopyrite geochronology. *Ore Geol Rev* 121:1–20
- Cheng XH, Yang FQ, Zhang R, Xu QF, Yang CD (2020b) Petrogenesis and geodynamic implications of early palaeozoic granitic rocks at the Hongshi Cu deposit in East Tianshan Orogenic Belt, NW China: constraints from zircon U–Pb geochronology, geochemistry, and Sr–Nd–Hf isotopes. *Geol J* 55:1890–1912
- Clayton RN, Mayeda TK (1963) The use of bromine pentafluoride in the extraction of oxygen from oxides and silicates for isotopic analysis. *Geochim Cosmochim Acta* 27:43–52
- Clayton RN, O’Neil JR, Mayeda TK (1972) Oxygen isotope exchange between quartz and water. *J Geophys Res* 77(17):3057–3067
- Coleman ML, Sheppard TJ, Durham JJ, Rouse JE, Moore GR (1982) Reduction of water with zinc for hydrogen isotope analysis. *Anal Chem* 54:993–995
- Daukeev SZH, Uzhkenov BS, Bespaev KhA, Miroshnichenko LA, Mazurov AK, Sayduakasov MA (2004) Atlas of mineral deposit models of the republic of Kazakhstan. Almaty, Printing House “Center for geoinformation of the Military Forces of the Republic of Kazakhstan”. pp 1–141
- Deng XH, Wang JB, Wang YW, Li YC, Fang TH, Mao QG (2014) Geological characteristics of the Hongshi Cu–Au deposit, eastern Tianshan, Xinjiang and discussion of the deposit genesis. *Mineral Exploration* 5(2):159–168
- Deng XH, Wang JB, Pirajno F, Wang YW, Li YC, Li C, Zhou LM, Chen YJ (2016) Re–Os dating of chalcopyrite from selected mineral deposits in the kalatag district in the eastern Tianshan orogen, China. *Ore Geol Rev* 77:72–81
- Deng XH, Chen YJ, Santosh M, Wang JB, Li C, Yue SW, Zheng Z, Chen HJ, Tang HS, Dong LH, Qu X (2017) U–Pb zircon, Re–Os molybdenite geochronology and Rb–Sr geochemistry from the Xiaobaishitou W (–Mo) deposit: implications for Triassic tectonic setting in eastern Tianshan, NW China. *Ore Geol Rev* 80:332–351
- Deng XH, Li YC, Xu QF, Liu Y, Zhang R, Li DD, Xu F (2018a) Discovery of the Jinling–Huangtan Au–Cu deposit in the Kalatag, eastern Tianshan Orogen and its significance. *Mineral Exploration* 9(7):1322–1333 (in Chinese with English abstract)
- Deng XH, Wang JB, Santosh M, Li YC, Wang YW, Mao QG, Long LL, Chen X (2018b) New <sup>40</sup>Ar/<sup>39</sup>Ar ages from the Kalatag VMS Deposits, eastern Tianshan, NW China: constraints on the timing of Cu mineralization and stratigraphy. *Ore Geol Rev* 100:250–262
- Deng XH, Wang JB, Santosh M, Wang YW, Long LL, Zhang HQ, Yang LY, Xu J, Chen X, Chen L (2018c) Early paleozoic volcanic rocks with VMS mineralization from eastern Tianshan orogen: implication for tectonic evolution. *Geol J* 53(5):2178–2192
- Deng XH, Wang JB, Pirajno F, Mao QG, Long LL (2020) A review of Cu-dominant mineral systems in the Kalatag district, East Tianshan, China. *Ore Geol Rev* 117(103284):1–27
- Eadington PJ, Smith JW, Wilkins RWT (1974) Fluid inclusion and sulphur isotope research, Mount Morgan, Queensland. Australasian Institute of Mining and Metallurgy, pp 441–444
- Franklin JM, Gibson HL, Jonasson IR, Galley AG (2005) Volcanogenic massive sulfide deposits. *Economic Geology, 100th Anniversary Volume*, pp 523–560

- Han CM, Zhao GC (2003) Major types and characteristics of the Late Paleozoic ore deposits, East Tianshan, Northwest China. *Int Geol Rev* 45:798–814
- Han CM, Xiao WJ, Zhao GC, Mao JW, Li SZ, Yan Z, Mao QG (2006a) Major types, characteristics and geodynamic mechanism of Upper Paleozoic copper deposits in northern Xinjiang, northwestern China. *Ore Geol Rev* 28(3):308–328
- Han CM, Xiao WJ, Zhao GC, Sun M, Qu WJ, Yang JM, Wang ZL, Yan Z, Mao QG (2006b) Geological characteristics and genesis of the Tuwu porphyry copper deposit, Hami, Xinjiang, Central Asia. *Ore Geol Rev* 29(4):472–472
- Han CM, Xiao WJ, Zhao GC, Qu WJ, Du AD (2007) Re–Os dating of the Kalatongke Cu–Ni deposit, Altay Shan, NW China, and resulting geodynamic implications. *Ore Geol Rev* 32(1–2):452–468
- Han CM, Xiao WJ, Zhao GC, Sun M, Qu WJ, Du AD (2010) In-Situ U–Pb, Hf and Re–Os isotopic analyses of the Xiangshan Ni–Cu–Co deposit in Eastern Tianshan (Xinjiang), Central Asia Orogenic Belt: constraints on the timing and genesis of the mineralization. *Lithos* 120:547–562
- He XH (2019) Metallogenesis of Huangtan Au–Cu deposit in Kalatag ore Concentration Area, East Tianshan. China University of Geosciences, Beijing, pp 1–64
- Hedenquist JW, Arribas A, Reynolds TJ (1998) Evolution of an intrusion-centered hydrothermal system; Far Southeast–Lepanto porphyry and epithermal Cu–Au deposits, Philippines. *Econ Geol* 93:373–404
- Herrington RJ, Scotney PM, Roberts S, Boyce AJ, Harrison D (2011) Temporal association of arc–continent collision, progressive magma contamination in arc volcanism and formation of gold-rich massive sulphide deposits on Wetar Island (Banda arc). *Gondwana Res* 19(3):583–593
- Hoefs J (2009) Stable isotope geochemistry, 6th edn. Springer, Berlin, pp 1–285
- Hou GS, Tang HF, Liu CQ (2006) Geochemical characteristics of the Late Paleozoic volcanics in Jueluotage tectonic belt, eastern Tianshan and its implications. *Acta Petrol Sin* 22(5):1167–1177 **(in Chinese with English abstract)**
- Hu RZ (1997) He, Ar isotopic geochemistry of ore–forming fluids. *Bull Mineral Petrol Geochem* 16(2):120–124 **(in Chinese without English abstract)**
- Huang JH, Chen HY, Han JS, Lu WJ, Zhang WF (2016) Spacial and temporal characteristics of mineralization and alteration zonation of the Honghai VMS Cu–Zn deposit in the Kalatag District, East Tianshan, NW China. *Geochimica* 45(6):582–600
- Huston DL (1999) Stable isotopes and their significance for understanding the genesis of volcanic-hosted massive sulfide deposits: a review. *Rev Econ Geol* 8:157–179
- Huston DL, Large RR (1989) A chemical model for the concentration of gold in volcanogenic massive sulphide deposits. *Ore Geol Rev* 4(3):171–200
- Kendrick MA, Burgess R, Patrick RAD, Turner G (2001) Fluid inclusion noble gas and halogen evidence on the origin of Cu porphyry mineralization fluids. *Geochim Cosmochim Acta* 65(16):2651–2668
- Kusakabe M, Robinson BW (1977) Oxygen and sulfur isotope equilibria in the  $\text{BaSO}_4\text{–HSO}_4\text{–H}_2\text{O}$  system from 110 to 350°C and applications. *Geochim Cosmochim Acta* 41(8):1033–1040
- Lawley C, Selby D, Imber J (2013) Re–Os molybdenite, pyrite, and chalcopyrite geochronology, Lupa gold field, southwestern Tanzania; tracing metallogenic time scales at mid-crustal shear zones hosting orogenic Au deposits. *Econ Geol* 108:1591–1613
- Li JY, Xiao WJ, Wang KZ, Sun GH, Gao LM (2003) Neoproterozoic–Paleozoic tectonostratigraphy, magmatic activities and tectonic evolution of eastern Xinjiang, NW China. In: Ma JW, Goldfarb RJ, Seltnann R, Wang DH, Xiao WJ, Hart C (eds) Tectonic evolution and metallogeny of the Chinese Altay and Tianshan. CERAMS, Natural History Museum, London, pp 31–74
- Li WQ, Wang R, Wang H, Xia B (2006) Geochemistry and petrogenesis of the Kalatag intrusion in the “Tuha window”. *Geol China* 33:559–565 **(in Chinese with English abstract)**
- Li C, Qu WJ, Zhou LM, Du AD (2010) Rapid separation of osmium by direct distillation with Carius tube. *Rock Mineral Anal* 29:14–16 **(in Chinese with English abstract)**
- Li W, Chen JL, Dong YP, Xu XY, Li ZP, Liu XM, He DF (2016) Early Paleozoic subduction of the Paleo–Asian Ocean: Zircon U–Pb geochronological and geochemical evidence from the Kalatag high–Mg andesites, East Tianshan. *Acta Petrol Sin* 32(2):505–552 **(in Chinese with English abstract)**
- Li N, Yang FQ, Zhang ZX (2020) Fluid inclusions and isotope (C, H, O, S, He, and Ar) study of the Xiaobaishitou skarn W–(Mo) deposit, East Tianshan, NW China. *Ore Geol Rev* 122:Article 103520 **(1–27)**
- Liang B (2018) Simple analysis about geological characteristics and ore genesis of the Huangtan Au–Cu polymetallic deposit in Hami, Xinjiang. *Xinjiang You Se Jinshu* 185(02):66–69 **(in Chinese with English abstract)**
- Liang WJ, Yan GS, Li JC, Zuo QC, Li YS (2016) Characteristics of fluid inclusions of the Xiaotieshan lead–zinc polymetallic deposit in Gansu province. *Bull Miner Petrol Geochem* 35(2):317–327 **(in Chinese with English abstract)**
- Lobanov K, Yakubchuk A, Creaser RA (2014) Besshi-Type VMS Deposits of the Rudny Altai (Central Asia). *Econ Geol* 109(5):1403–1430
- Long LL, Wang JB, Wang YW, Mao QG, Deng XH, Zhao LT, Sun ZY, Sun Y, Gao YH (2016) Discussion on the age of ore-host volcanic strata in the Kalatage ore concentration area, eastern Tianshan: evidence from SHRIMP zircon U–Pb dating. *Mineral Exploration* 7:31–37 **(in Chinese with English abstract)**
- Long LL, Wang JB, Wang YW, Fang TH, Mao QG, Gao YH, Zhao LT, Gao LM (2017) Geochronological, geochemical characteristics and potential mineralization significance of the rhyolite in Kalatage copper polymetallic ore cluster area, eastern Tianshan. *Acta Petrol Sin* 33(2):367–384 **(in Chinese with English abstract)**
- Ludwig KR (2003) ISOPLOT 3.0.0: a geochronological toolkit for Microsoft excel. Berkeley Geochronology Center, Berkeley
- Luo T, Liao QA, Zhang XH, Chen JP, Wang GC, Huang X (2016) Geochronology and geochemistry of Carboniferous metabasalts in eastern Tianshan, Central Asia: evidence of a back-arc basin. *Int Geol Rev* 58(6):756–772
- Mamyrin BA, Tolstikhin IN (1984) Helium isotopes in nature. Elsevier, Amsterdam, pp 38–169
- Mao JW, Kerrich R, Li HY, Li YH (2002) High  $^3\text{He}/^4\text{He}$  ratios in the Wangu gold deposit, Hunan province, China: implications for mantle fluids along the Tanlu deep fault zone. *Geochem J* 36:197–208
- Mao QG, Fang TH, Wang JB, Wang SL, Wang N (2010) The geochronology studies of the early Paleozoic Honghai massive sulfide deposits and its geological significance, Kalatage belt in eastern Tianshan Mountain, Xinjiang, Northwest China. *Acta Petrol Sin* 26:3017–3026 **(in Chinese with English abstract)**
- Mao QG, Wang JB, Fang TH, Yu MJ, Huang XK, Wang N (2014) Study on Metallogenesis of Early Paleozoic VMS deposits in the Honghai, Kalatag, East Tianshan. *Mineral Deposits* S1:429–430 **(in Chinese with English abstract)**
- Mao YJ, Qin KZ, Li CS, Tang DM (2015a) A modified genetic model for the Huangshandong magmatic sulfide deposit in the central Asian Orogenic Belt, Xinjiang, Western China. *Miner Deposita* 50:65–82
- Mao QG, Wang JB, Fang TH, Zhu JJ, Fu WW, Yu MJ, Huang XK (2015b) Lead and sulfur isotope studies of sulfides from Honghai VMS–type deposit in Kalatage ore belt of eastern Tianshan



- Mountains. *Mineral Deposits* 34(4):730–744 (**in Chinese with English abstract**)
- Mao QG, Wang JB, Fang TH, Yu MJ, Zhu JJ, Zhang R, Fu WW, Gao WH (2016) Geological characteristics of Honghai VMS type deposit of Kalatage ore belt and discussion of deposit genesis type in the eastern Tianshan. *Mineral Exploration* 7(1):17–30 (**in Chinese with English abstract**)
- Mao QG, Yu MJ, Xiao WJ, Windley BF, Li YC, Wei XF, Zhu JJ, Lü XQ (2018) Skarn-mineralized porphyry adakites in the Harlik arc at Kalatage, E. Tianshan (NW China): Slab melting in the Devonian-early Carboniferous in the southern Central Asian Orogenic Belt. *J Asian Earth Sci* 153:365–378
- Mao QG, Wang JB, Xiao WJ, Windley BF, Schulmann K, Yu MJ, Fang TH, Li YC (2019) Mineralization of an intra-oceanic arc in an accretionary orogen: insights from the Early Silurian Honghai volcanogenic massive sulfide Cu–Zn deposit and associated adakites of the Eastern Tianshan (NW China). *Geol Soc Am Bull* 131(5–6):803–830
- Mao QG, Wang JB, Yu MJ, Ao SJ, Deng XH, Lü XQ, Li YC (2020) Re–Os and U–Pb geochronology for the Xiaorequanzi VMS deposit in the Eastern Tianshan, NW China: constraints on the timing of mineralization and stratigraphy. *Ore Geol Rev* 122:Article 103473 (**1–14**)
- Mao QG (2014) The geological, metallogenesis and metallogenic prognosis studies of the Kalatage copper polymetallic ore district in eastern Tianshan, NW China. Post Doctoral Research Report, pp. 1–154 (**in Chinese with English abstract**)
- Marty B, Jambon A, Sano Y (1989) Helium isotope and CO<sub>2</sub> in volcanic gases of Japan. *Chem Geol* 76:25–40
- Meisel T, Walker RJ, Morgan JW (1996) The osmium isotopic composition of the Earth's primitive upper mantle. *Nature* 383(6600):517–520
- Mercier-Langevin P, Hannington MD, Dubé B, Bécu V (2011) The gold content of volcanogenic massive sulfide deposits. *Miner Deposita* 46(5):509–539
- Nozaki T, Kato Y, Suzuki K (2010) Re–Os geochronology of the Iimori Besshi-type massive sulfide deposit in the Sanbagawa metamorphic belt, Japan. *Geochim Et Cosmochim Acta* 74(15):4322–4331
- Ohmoto H, Rye RO (1979) Isotopes of sulfur and carbon. In: Barnes HL (ed) *Geochemistry of hydrothermal ore deposits*, seconded. Wiley, New York, pp 509–567
- Ohmoto H, Tanimura S, Date J, Takahashi T (1983) Geologic setting of the kuroko deposits, Japan: Part I. Geologic history of the Green tuff region. Part II. Stratigraphy and structure of the Hokuroku district. Part III. Submarine Calderas and Kuroko Genesis: *Economic Geology Monograph* 5:9–54
- Palmer MR, Turekian KK (1986) 187Os/188Os in marine manganese nodules and the constraints on the crustal geochemistries of rhenium and osmium. *Nature* 319(6050):216–220
- Patten CGC, Pitcairn IK, Teagle DAH, Harris M (2015) Mobility of Au and related elements during the hydrothermal alteration of the oceanic crust: implications for the sources of metals in VMS deposits. *Miner Deposita* 51:179–200
- Qin KZ, Su BX, Sakyi PA, Tang DM, Li XH, Sun H, Xiao QH, Liu PP (2011) SIMS zircon U–Pb geochronology and Sr–Nd isotopes of Ni–Cu-bearing mafic–ultramafic intrusions in eastern Tianshan and Beishan in correlation with flood basalts in Tarim Basin (NW China): constraints on a ca. 280 Ma mantle plume. *Am J Sci* 311:237–260
- Qu WJ, Du AD (2003) Highly precise Re–Os dating of molybdenite by ICP–MS with Carius tube sample digestion. *Rock Miner Anal* 22:254–262 (**in Chinese with English abstract**)
- Qu WJ, Du AD, Li C, Sun WJ (2009) High-precision determination of osmium isotopic ratio in the Jinchuan copper–nickel sulfide ore samples. *Rock Miner Anal* 28:219–222 (**in Chinese with English abstract**)
- Robinson B, Kusakabe M (1975) Quantitative preparation of sulphur dioxide for <sup>34</sup>S/<sup>32</sup>S analyses from sulphides by combustion with cuprous oxide. *Anal Chem* 47:1179
- Roedder E (1984) Fluid inclusions. *Rev Mineral* 12:646
- Sano Y, Wakita H (1985) Geographical distribution of <sup>3</sup>He/<sup>4</sup>He in Japan: implications for tectonics and incipient magmatism. *J Geophys Res* 90:8729–8741
- Seal RR, Alpers CN, Rye RO (2000) Stable isotope systematics of sulfate minerals. *Rev Miner Geochem* 40(1):541–602
- Sengör AMC, Natalin BA, Burtman VS (1993) Evolution of the Altaid tectonic collage and Paleozoic crustal growth in Eurasia. *Nature* 364:299–307
- Seward TM (1973) Thio complexes of gold and the transport of gold in hydrothermal ore solutions. *Geochim Cosmochim Acta* 37(3):379–399
- Seward TM (1984) The transport and deposition of gold in hydrothermal systems. In Foster, R.P., *Gold '82: the geology, geochemistry and genesis of gold deposits*. *Geol Soc Zimbabwe Spec Pub* 1:165–181
- Shanks WC (2001) Stable isotopes in seafloor hydrothermal systems: vent fluids, hydrothermal deposits, hydrothermal alteration, and microbial processes. *Rev Mineral Geochem* 43(1):469–525
- Sheppard SM (1986) Characterization and isotopic variations in natural waters. *Rev Mineral* 16(1):165–183
- Sherlock RL, Roth T, Spooner ETC, Bray CJ (1999) Origin of the Eskay Creek precious metal-rich volcanogenic massive sulfide deposit: fluid inclusion and stable isotope evidence. *Econ Geol* 94(6):803–824
- Simmons SF, Sawkins FJ, Schlutter DJ (1987) Mantle-derived helium in two Peruvian hydrothermal ore deposits. *Nature* 329:429–432
- Simmons SF, White NC, John D (2005) Geological characteristics of epithermal precious and base metal deposits. *Econ Geol* 100:485–522
- Solomon M, Eastoe CJ, Walshe JL, Green GR (1988) Mineral deposits and sulphur isotope abundances in the Mount Read Volcanics between Que River and Mount Darwin, Tasmania. *Econ Geol* 83:1307–1328
- Song SM, Hu K, Jiang SY, Li K (2007) The He–Ar–Pb–S isotope tracing on ore-forming fluid in dabao hill polymetallic deposit, North Guangdong. *Contrib Geol Miner Resour Res* 22(2):87–99 (**in Chinese with English abstract**)
- Stein HJ, Hannah JL (2014) The emerging potential of Re–Os isotope geochemistry for source rocks and maturation-migration histories. *Int Pet Technol Confer* 17693:1–5
- Stuart FM, Turner G, Duckworth RC, Fallick AE (1994) Helium isotopes as tracers of trapped hydrothermal fluids in ocean–floor sulfides. *Geology* 22:823–826
- Stuart FM, Burnard PG, Taylor RP, Turner G (1995) Resolving mantle and crustal contributions to ancient hydrothermal fluids: He–Ar isotopes in fluid inclusions from Dae Hwa W–Mo mineralization, South Korea. *Geochim Cosmochim Acta* 59:4663–4673
- Sun Y, Wang JB, Li YC, Wang YW, Yu MJ, Long LL, Lü XQ, Chen L (2018) Recognition of Late Ordovician Yudai porphyry Cu (Au, Mo) mineralization in the Kalatag district, Eastern Tianshan terrane, NW China Constraints from geology, geochronology, and petrology. *Ore Geol Rev* 100:220–236
- Sun Y, Wang JB, Lü XQ, Yu MJ, Li YC, Mao QQ, Wang YW, Long LL (2019) Geochronology, petrogenesis and tectonic implications of the newly discovered Cu–Ni sulfide-mineralized Yueyawan gabbroic complex, Kalatag district, northwestern Eastern Tianshan, NW China. *Ore Geol Rev* 109:598–614
- Sun BK, Ruan BX, Lv XB, Tuohan B, Ratchford ME (2020) Geochronology and geochemistry of the igneous rocks and ore-forming age in the Huangtan Au–Cu deposit in the Kalatag district, Eastern Tianshan, NW China: Implications for petrogenesis, geodynamic setting, and mineralization. *Lithos* 368–369:105594

- Taylor HP (1974) The application of oxygen and hydrogen isotope studies to problems of hydrothermal alterations and ore deposition. *Econ Geol* 69:843–883
- Turner G, Burnard PG, Ford JL, Gilmour JD, Lyon IC, Stuart FM (1993) Tracing fluid sources and interaction. *Philos Trans R Soc A Math Phys Eng Sci* 344:127–140
- Ulrich T, Golding SD, Kamber BS, Zaw K, Taube A (2002) Different mineralization styles in a volcanic-hosted ore deposit: the fluid and isotopic signatures of the Mt. Morgan Au–Cu deposit, Australia. *Ore Geol Rev* 22(1):61–90
- Walker RJ, Morgan JW (1989) Rhenium-osmium isotope systematics of carbonaceous chondrites. *Science* 343(4890):519–522
- Wang YH, Zhang FF (2016) Petrogenesis of early Silurian intrusions in the Sanchakou area of Eastern Tianshan, Northwest China, and tectonic implications: Geochronological, geochemical, and Hf isotopic evidence. *Int Geol Rev* 58(10):1294–1310
- Wang JB, Wang YW, He ZH (2006) Ore deposits as a guide to the tectonic evolution in the East Tianshan Mountains NW China. *Geol China* 33:461–469 (in Chinese with English abstract)
- Wang YH, Zhang FF, Liu JJ, Xue CJ, Li BC, Xian XC (2018a) Ore genesis and hydrothermal evolution of the Donggebi porphyry Mo deposit, Xinjiang, Northwest China: evidence from isotopes (C, H, O, S, Pb), fluid inclusions, and molybdenite Re–Os dating. *Econ Geol* 113:463–488
- Wang YF, Chen HY, Han JS, Chen SB, Huang BQ, Li C, Tian QL, Wang C, Xu JX, Chen MX (2018b) Paleozoic tectonic evolution of the Dananhu-Tousuquan island arc belt, Eastern Tianshan: constraints from the magmatism of the Yuhai porphyry Cu deposit, Xinjiang, NW China. *J Asian Earth Sci* 153:282–306
- Windley BF, Alexeiev D, Xiao WJ, Kroner A, Badarch G (2007) Tectonic models for accretion of the Central Asian Orogenic Belt. *J Geol Soc* 164:31–47
- Xiao WJ, Zhang LC, Qin KZ, Sun S, Li JL (2004) Paleozoic accretionary and collisional tectonics of the eastern Tianshan (China): implications for the continental growth of Central Asia. *Am J Sci* 304(4):370–395
- Xiao WJ, Windley BF, Allen MB, Han CM (2013) Paleozoic multiple accretionary and collisional tectonics of the Chinese Tianshan orogenic collage. *Gondwana Res* 23:1316–1341
- Xiao WJ, Han CM, Liu W, Wan B, Zhang JE, Ao SJ, Zhang ZY, Song DF, Tian ZH, Luo J (2014) How many sutures in the southern Central Asian Orogenic Belt: insights from East Xinjiang–West Gansu (NW China)? *Geosci Front* 5:525–536
- Xiao WJ, Windley B, Sun S, Li JL, Huang BC, Han CM, Yuan C, Sun M, Chen HL (2015) A tale of amalgamation of three Permian–Triassic collage systems in Central Asia: oroclinal sutures, and terminal accretion. *Annu Rev Earth Planet Sci* 43:477–507
- Xiao B, Chen HY, Hollings P, Han JS, Wang YF, Yang JT, Cai KD (2017) Magmatic evolution of the Tuwu–Yandong porphyry Cu belt, NW China: constraints from geochronology, geochemistry and Sr–Nd–Hf isotopes. *Gondwana Res* 43:74–91
- Xie GQ, Mao JW, Li W, Zhu QQ, Liu HB, Jia GH, Li YH, Li JJ, Zhang J (2016) Different proportion of mantle-derived noble gases in the Cu–Fe and Fe skarn deposits: He–Ar isotopic constraint in the Edong district, Eastern China. *Ore Geol Rev* 72:343–354
- Xu J (2017) Geological and geochemical characteristics of Ore-Hosting Strata in the Kalatag Ore Concentration Area, Xinjiang. China University of Geosciences, Beijing, pp 1–69 (in Chinese with English abstract)
- XXMCL (Xinjiang Xituo Mining Co. Ltd) (2019) Detailed Investigation Report of Huangtan Gold, Copper and Zinc deposit in Hami City, Xinjiang (in Chinese)
- Yakubchuk AS, Shatov VV, Kirwin D, Edwards A, Tomurtogoo O, Badarch G, Buryak VA (2005) Gold and base metal metallogeny of the Central Asian Orogenic Supercollage. *Econ Geol* 100:1035–1068
- Yang CD (2017) Metallogenesis of the Sarsuk polymetallic Au deposit in Altay, Xinjiang. Chinese Academy of Geological Sciences, Beijing, pp 1–191 (in Chinese with English abstract)
- Yang CD, Chai FM, Yang FQ, Santosh M, Xu QF, Wang W (2018a) Genesis of the Huangtupo Cu–Zn deposit in the eastern Tianshan, NW China: constraints from geology, Rb–Sr and Re–Os geochronology, fluid inclusions, and H–O–S–Pb isotopes. *Ore Geol Rev* 101:725–739
- Yang FQ, Li Q, Yang CD, Zhang ZX (2018b) A combined fluid inclusion and S–H–O–He–Ar isotope study of the Devonian Ashele VMS-type copper–zinc deposit in the Altay orogenic belt, Northwest China. *J Asian Earth Sci* 161:139–163
- Ye XT, Zhu WG, Zhong H, He DF, Ren T, Bai ZJ, Fan HP, Hu WJ (2013) Zircon U–Pb and chalcopyrite Re–Os geochronology, REE geochemistry of the Yinachang Fe–Cu–REE deposit in Yunnan Province and its geological significance. *Acta Petrol Sin* 29:1167–1186 (in Chinese with English abstract)
- Ying LJ, Wang CH, Tang JX, Wang DH, Qu WJ, Li C (2014) Re–Os systematics of sulfides (chalcopyrite, bornite, pyrite and pyrrhotite) from the Jiama Cu–Mo deposit of Tibet. *China J Asian Earth Sci* 79:497–506
- Yu X (2014) Geochemistry of Volcanic Rocks in Huangtupo VMS Cu Polymetallic Deposit in Eastern Tianshan, Xinjiang. Xinjiang University, Urumqi, pp 1–36 (in Chinese with English abstract)
- Yu MJ, Wang YW, Wang JB, Mao QG, Deng XH, Sun Y, Zhang R (2019) The mineralization of the Kalatage arc, Eastern Tianshan, NW China: Insights from the geochronology of the Meiling Cu–Zn(Au) deposit. *Ore Geol Rev* 107:72–86
- Yu MJ, Wang JB, Mao QG, Sun Y, Zhang R, Tian J, Guo WD (2020) Geochemical characteristics of Late Carboniferous mineralization in the East Tianshan: a case study of the Meiling deposit in the Kalatage area. *Ore Geol Rev* 117:Article 103285 (1–18)
- Zaw K, Gemmill JB, Large RR, Mernagh TP, Ryan CG (1996) Evolution and source of ore fluids in the stringer system, Hellyer VHMS deposit, Tasmania, Australia: evidence from fluid inclusion microthermometry and geochemistry. *Ore Geol Rev* 10(3–6):251–278
- Zaw K, Hunns SR, Large RR, Gemmill JB, Ryan CG, Mernagh TP (2003) Microthermometry and chemical composition of fluid inclusions from the Mt. Chalmers volcanic-hosted massive sulfide deposit, central Queensland, Australia: implications for ore genesis. *Chem Geol* 194(1–3):225–244
- Zeng ZG, Qin YS, Zhai SK (2000) He, Ne and Ar isotope compositions of fluid inclusions in hydrothermal sulfides from the TAG hydrothermal field mid-Atlantic ridge. *Sci China (ser d)* 44(3):221–228 (in Chinese with English abstract)
- Zheng JH, Chai FM, Feng WY, Yang FQ, Shen P (2018) Geochemistry and chronology of the early Paleozoic diorites and granites in the Huangtupo volcanogenic massive sulfide (VMS) deposit, Eastern Tianshan, NW China: Implications for petrogenesis and geodynamic setting. *Lithos* 302–303:455–466
- Zhou LM, Gao BY, Wang LB, Li C, Qu WJ, Hou ZQ, Du AD (2012) Improvements on the separation method of osmium by direct distillation in Carius tube. *Rock Miner Anal* 31:413–418 (in Chinese with English abstract)
- Zhu ZM, Sun YL (2013) Direct Re–Os dating of chalcopyrite from the Lala IOCG deposit in the Kangdian copper belt, China. *Econ Geol* 108:871–882